Check for updates

Advanced Materials

ADVANCED MATERIALS
www.advmat.de

RESEARCH ARTICLE

Polysaccharide Engineered Nanozymes Target Inflammation for Alleviating Colitis-Associated Mental Disorders via Microbiome-Gut–Brain Axis

Gen Wei[1,2] | Hui Zhang[1] | Shuang Zhao[1] | Jian Jiang[1] | Chen Liu[3] | Peng Li[1] | Yaya Ni[1] | Hua Dai[1] | Lei Fan[4] | Hui Wei[5] | Juqun Xi[1,2]

[1]School of Traditional Chinese Medicine, Faculty of Medicine, Yangzhou University, Yangzhou, Jiangsu, China | [2]Key Laboratory of the Jiangsu Higher Education Institutions for Integrated Traditional Chinese and Western Medicine in Senile Diseases Control (Yangzhou University), Yangzhou, Jiangsu, China | [3]Northern Jiangsu People's Hospital Affiliated to Yangzhou University, Yangzhou, Jiangsu, China | [4]School of Chemistry & Materials, Yangzhou University, Yangzhou, Jiangsu, China | [5]Department of Biomedical Engineering, College of Engineering and Applied Sciences, Nanjing National Laboratory of Microstructures, Jiangsu Key Laboratory of Artificial Functional Materials, Nanjing University, Nanjing, Jiangsu, China

Correspondence: Lei Fan (fanlei@yzu.edu.cn) | Hui Wei (weihui@nju.edu.cn) | Juqun Xi (xijq@yzu.edu.cn)

Received: 5 November 2025 | **Revised:** 25 January 2026 | **Accepted:** 26 January 2026

Keywords: colitis-associated mental disorders | gut inflammation | gut microbiota-derived metabolism | microbiome-gut–brain axis | polysaccharide engineered nanozymes

ABSTRACT

Molecular therapies for colitis-associated mental disorders show limited efficacy because they usually focus on a single pathway and exhibit substantial off-target toxicity toward healthy tissues. To tackle this limitation, bioinformatic approaches are employed to predict that inflammation and metabolism may be potential targets for Fucoidan. Guided by this prediction, we develop oral polysaccharide engineered nanozymes, Fucoidan-cerium nanocomplexes (FucCeNCs), which are capable of targeting the inflamed colon through electrostatic interactions, exerting anti-inflammatory effects, and concurrently regulating gut microbiota-derived metabolism. In a murine model of ulcerative colitis-associated mental disorders, FucCeNCs show anti-inflammatory and gut barrier-protective effects, thereby suppressing microglial/astrocytic overactivation and preserving neuronal integrity through the transmission of anti-inflammatory cytokines via gut–brain axis. Importantly, FucCeNCs restore gut microbial homeostasis through increasing the relative abundance of probiotics and reducing proportions of pathogens. This shift results in a marked attenuation of abnormal amino acid biosynthesis and metabolism in fecal metabolites, which in turn leads to elevated levels of bioactive metabolites such as homovanillic acid and γ-aminobutyric acid. These metabolites ultimately attenuate neuroinflammation via the microbiome-gut–brain axis, ameliorating depression- and anxiety-like behaviors. These results identify microbiome-gut–brain axis as pivotal therapeutic target for colitis-associated mental disorders therapy, which can be addressed by polysaccharide engineered nanozymes.

1 | Introduction

Mental disorders, characterized by clinically significant disturbances in cognition, emotion, and behavior, occur in approximately 1.1 billion people (nearly 1 in every 7 people) around the world. Anxiety and depression are the most prevalent types, and their increasing incidence among adolescents and young adults has become an important public health issue worldwide

Gen Wei and Hui Zhang contributed equally to this work.

© 2026 Wiley-VCH GmbH

[1–3]. The etiology of mental disorders is multifactorial, involving a complex interplay of genetic predisposition, neurochemical and functional imbalances in the brain (e.g., neurotransmitters), as well as adverse life experiences and environmental factors such as abuse, trauma, significant stress, social isolation, and traumatic brain injury. In addition, the presence of a chronic or serious medical condition is a recognized risk factor for developing mental disorders [4, 5]. A pertinent example is inflammatory bowel disease (IBD), including Crohn's disease and ulcerative colitis (UC) [6–9], which is associated with a high prevalence of neuropsychiatric comorbidities, affecting nearly one-quarter of patients with depression and one-third with anxiety [10, 11]. This clinical correlation is driven via microbiome-gut–brain axis, where gut immune inflammation, microbial dysbiosis, and impaired vagal signaling converge to create a bidirectional pathophysiological link with mental disorders [10, 12–15]. Therefore, it is urgent to explore therapeutic strategies for colitis-associated mental disorders via microbiome-gut–brain axis.

Currently, the clinical drug intervention such as aminosalicylates, corticosteroids, immunosuppressants, and antidepressants [16, 17] usually focus on a single therapeutic pathway, resulting in unsatisfactory efficacy. Moreover, long-term use of these drugs often comes with adverse reactions and significant non-targeted toxicity to normal tissues. Consequently, these modalities demonstrate poor effectiveness in addressing colitis-associated mental disorders [17, 18]. Pathologically, the excessive production of reactive nitrogen and oxygen species (RNOS) mediates oxidative stress and drives inflammatory processes via gut–brain axis. Concurrently, an imbalance in the gut microbiota also reduces the production of beneficial microbial metabolites, thereby contributing to neuroinflammation via microbiota-gut–brain axis [7, 8, 19]. We reason that a targeting strategy capable of localizing treatment to inflammatory sites while integrating antioxidant and anti-inflammatory actions with the modulation of gut microbial homeostasis would be a promising therapeutic strategy.

Metal-based nanozymes, inspired by superoxide dismutase (SOD), effectively scavenge RNOS to break the cycle of oxidative stress and inflammation [20–27]. However, their inability to regulate gut microbial homeostasis limits their efficacy against colitis-associated mental disorders. To address this, polysaccharides are integrated as prebiotic components that modulate gut microbiota [28, 29], while their abundant functional groups chelate metal ions to form catalytic nanocomplexes [30–35]. Notably, Fucoidan, a sulfated polysaccharide, exhibits a strong negative charge for targeted binding to inflamed colonic sites and provides additional metal-coordination sites [36]. Given the exceptional RNOS-scavenging capacity of cerium-based nanozymes via Ce^{3+}/Ce^{4+} redox cycling [26, 37], we hypothesize that Fucoidan engineered nanozymes, Fucoidan-cerium nanocomplexes (designated as FucCeNCs) represent a synergistic strategy for treating colitis-associated mental disorders. To validate our hypothesis, we constructed FucCeNCs via a straightforward chelation strategy. Upon oral delivery, FucCeNCs accumulate in the inflamed colon and execute a dual-mode therapeutic action: the Ce ions scavenge RNOS to drive macrophage polarization from a pro-inflammatory M1 to an anti-inflammatory M2 phenotype, while the Fucoidan component functions as a prebiotic to restore gut microbial homeostasis. The resulting anti-inflammatory cytokines and microbiota-derived metabolites then relay signals via microbiome-gut–brain axis. This coordinated communication effectively suppresses neuroinflammation by concurrently inhibiting cerebral glial activation and preserving neuronal integrity (Figure 1). Our design paves the way for the development of advanced polysaccharide engineered nanozymes to treat colitis-associated mental disorders via microbiome-gut–brain axis by simultaneously exerting anti-inflammatory effects and regulating gut microbiota-derived metabolism, especially bioactive metabolites.

2 | Results and Discussion

2.1 | Landscape of Genes Co-Expressed in Fucoidan, UC, and Depression

Studies have demonstrated that polysaccharides with negative charges can target the positively charged inflamed colonic tissues through electrostatic interactions [38]. Based on this rationale, Fucoidan was selected for the synthesis of FucCeNCs after our preliminary screening study. Compared with other bioactive polysaccharides (i.e., *Radix Paeoniae Alba* polysaccharide (RP) and *Bletilla Striata* polysaccharide (BP)), Fucoidan exhibited the strongest negative charge, as determined by zeta potential analysis (Figure 2a).

Importantly, Fucoidan is comprised of seven monosaccharides: L-Fucose, α-Rhamnose, D-Arabinose, D-Xylose, D-Mannose, D-Galactose, and D(+)-Glucose. Utilizing the Comparative Toxicogenomics Database (CTD), we systematically screened bioactive targets for each monosaccharide. Following the removal of duplicate entries, a total of 3,013 potential bioactive targets were identified (green circle). Subsequently, disease-related targets were collected from GeneCards, yielding 525 and 950 targets for depression (blue circle) and UC (pink circle), respectively (Figure 2b). Notably, 66 overlapping shared differentially expressed genes (DEGs) were identified, representing potential key mediators of Fucoidan's multiple therapeutic effects. Protein-Protein Interaction (PPI) network analysis (STRING Database; Homo sapiens; confidence > 0.4;) identified top 10 hub targets by node degree: IL6, TNF, ADIPOQ, AKT1, ALB, CCL2, IGF1, IL1β, IL10, and LEP (Figure 2c,d). These targets predominantly regulated inflammatory responses (IL family), metabolic homeostasis (ADIPOQ, LEP), and cell survival pathways (AKT1). Gene Ontology (GO) enrichment analysis highlighted critical biological processes, including interleukin-1 receptor ligand activity, antioxidant regulation, and interleukin-18 mediated signaling pathway (Figure 2e). Kyoto Encyclopedia of Genes and Genomes (KEGG) pathway analysis revealed significant enrichment in IL-17 signaling, adipocytokine signaling, and phosphoinositide 3-kinas-Protein kinase B (PI3K-Akt) pathways (Figure 2f), all of which were closely involved in inflammation and metabolism. Therefore, inflammation and metabolism may be potential targets for Fucoidan in the treatment of colitis-associated mental disorders.

15214095, 0, Downloaded from https://advanced.onlinelibrary.wiley.com/doi/10.1002/adma.202532010 by Nanjing University, Wiley Online Library on [13/02/2026]. See the Terms and Conditions (https://onlinelibrary.wiley.com/terms-and-conditions) on Wiley Online Library for rules of use; OA articles are governed by the applicable Creative Commons License

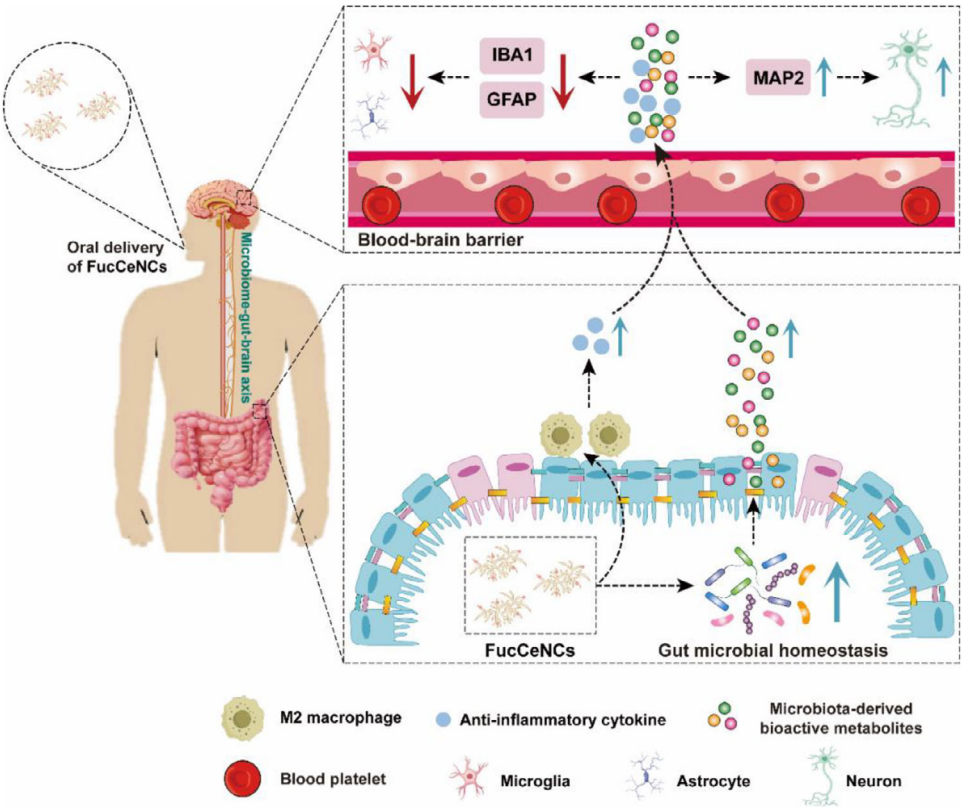

FIGURE 1 | Schematic illustration of the oral FucCeNCs with anti-inflammatory effects and gut microbiota-derived metabolism regulation via microbiota-gut–brain axis for the treatment of colitis-associated mental disorders. In the inflamed colon, the Ce ions performed the function as part of FucCeNCs, rather than free ionic states.

2.2 | Preparation and Characterization of FucCeNCs

On the basis of the above results, we used Fucoidan and $Ce(NO_3)_3$ as precursors to synthesize FucCeNCs through chelation-driven assembly (Figure S1). Dynamic light scattering (DLS) analysis showed that FucCeNCs had a unimodal size distribution with an average hydrodynamic diameter of 140 nm, significantly smaller than that of pure Fucoidan (220 nm) (Figure S2). Transmission electron microscopy (TEM) imaging confirmed the uniform size of FucCeNCs (~30 nm) (Figure 3a; Figure S3). Additionally, a distinct Tyndall effect was observed, further corroborating the colloidal nature of FucCeNCs (Figure 3a). The hydrodynamic diameter of FucCeNCs exhibited negligible change over 7 days in Dulbecco's Modified Eagle Medium (DMEM), deionized water, and 0.9% NaCl, demonstrating excellent colloidal stability (Figure S4). Then, we conducted powder X-ray diffraction (PXRD), Fourier transform infrared (FTIR), ultraviolet-visible (UV–vis) spectrophotometer, and X-ray spectroscopy (XPS) analyses to assess the composition and structure of FucCeNCs. As shown in Figure S5, both pure Fucoidan and FucCeNCs displayed a single broad diffraction peak, with no discernible peaks corresponding to crystalline $Ce(NO_3)_3$, indicating all Ce ions were chelated with Fucoidan. FTIR analysis revealed characteristic absorption bands at 3400 cm^{-1} (O–H), 1035 cm^{-1} (C–O–C), 1225 cm^{-1} (S = O), and 845 cm^{-1} (C–O–S) [39, 40], confirming the retention of Fucoidan's main structural components in FucCeNCs (Figure 3b). Meanwhile, the UV-vis spectrum of FucCeNCs was studied. Figure 3c shows that FucCeNCs had profile similar to free Fucoidan in the 230–400 nm range, with an additional broad absorption peak at 253 nm corresponding to Ce ions before ethylene diamine tetraacetic acid (EDTA) treatment. In contrast, following EDTA treatment, this characteristic peak vanished (Figure S6), further demonstrating the chelation between Ce ions and Fucoidan. In addition, we analyzed the surface chemical composition and electronic state of FucCeNCs by XPS. The XPS survey spectrum (Figure S7) showed typical peaks of C 1*s*, N 1*s*, O 1*s*, Ce 3*d*, and S 2*p*. The high-resolution C 1*s* XPS spectrum showed the presence of C–Ce, C–C, and C–O at 283.0, 284.8, and 286.4 eV, respectively (Figure S8a). The O 1*s* XPS spectrum could be deconvoluted into three peaks at 530.1, 531.0, and 531.7 eV (Figure S8b), which corresponded to Ce–O, O = C, and C–O–Ce. For Ce 3*d*, the Ce^{3+} content was determined to be 56.18%, while that of the Ce^{4+} was 43.80% (Figure 3d). The trivalent-to-tetravalent ratio of cerium atoms in FucCeNCs determined its enzyme-like activity. The above results showed the successful synthesis of FucCeNCs.

For effective electrostatic targeting of the inflamed colon, the negative charge of Fucoidan should be retained after chelation with Ce ions. Therefore, we measured the zeta potentials of Fucoidan and FucCeNCs. Figure 3e shows that Fucoidan had a negative charge of −41.43 ± 3.88 mV, while that of FucCeNCs remained negatively charged (−43.87 ± 2.76 mV). To evaluate the retention of FucCeNCs after oral administration in inflamed colonic tissues, fluorescence imaging was performed. The results demonstrated that Rhodamine B (RB)-labeled FucCeNCs exhibited a sustained fluorescence signal in the colon, with a detectable signal still observed at 12 h (Figure 3f,g), indicating the efficient

15214095, 0, Downloaded from https://advanced.onlinelibrary.wiley.com/doi/10.1002/adma.202522010 by Nanjing University, Wiley Online Library on [13/02/2026]. See the Terms and Conditions (https://onlinelibrary.wiley.com/terms-and-conditions) on Wiley Online Library for rules of use; OA articles are governed by the applicable Creative Commons License

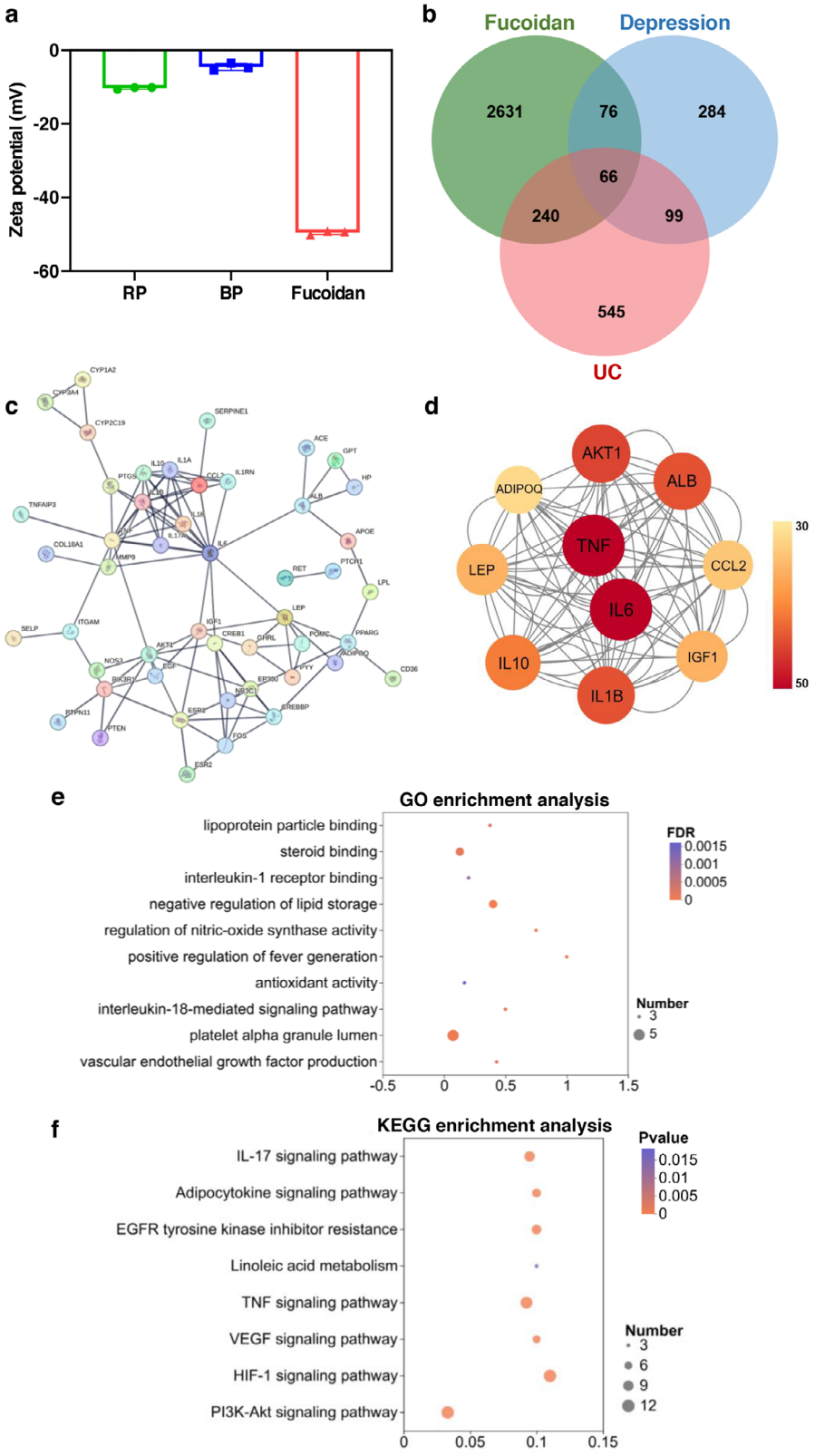

FIGURE 2 | Identification of targets associated with Fucoidan, UC, and depression from databases. (a) Zeta potentials of RP, BP, and Fucoidan. (b) Gene overlap among Fucoidan, UC, and depression. (c,d) Functional gene clusters identified in PPI networks (c), including top 10 enriched proteins: the two most highly enriched nodes, IL-6 and TNF, were given central prominence, while the remaining eight nodes were arranged alphabetically (d). (e) GO enrichment analysis of DEGs showing the top ten significantly enriched biological processes. (f) KEGG pathway enrichment analysis of DEGs (top 8 enriched pathways).

15214095, 0, Downloaded from https://advanced.onlinelibrary.wiley.com/doi/10.1002/adma.202522010 by Nanjing University, Wiley Online Library on [13/02/2026]. See the Terms and Conditions (https://onlinelibrary.wiley.com/terms-and-conditions) on Wiley Online Library for rules of use; OA articles are governed by the applicable Creative Commons License

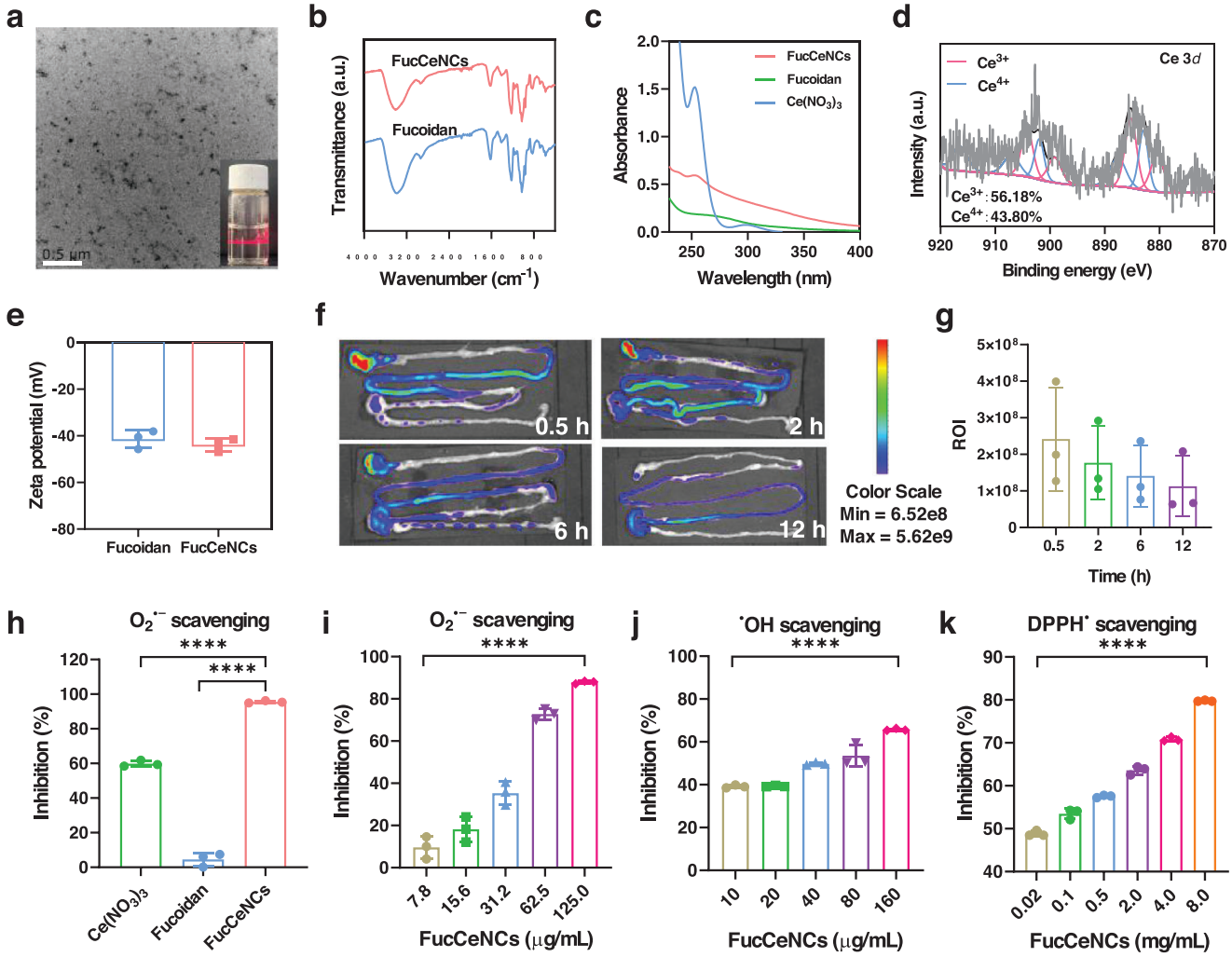

FIGURE 3 | Characterization of FucCeNCs. (a) TEM image of FucCeNCs. Inset: Tyndall scattering of FucCeNCs. Scale bar, 0.5 μm. (b) FTIR of FucCeNCs and Fucoidan. (c) UV–vis absorption spectra of FucCeNCs, Fucoidan, and $Ce(NO_3)_3$, respectively. (d) High-resolution Ce 3*d* peaks of FucCeNCs. (e) Zeta potentials of Fucoidan and FucCeNCs. (f,g) Fluorescent images (f) and the corresponding quantification (g) of fluorescence intensity with RB labeled FucCeNCs in inflamed colonic tissues. (h) Comparison of SOD-like activity among $Ce(NO_3)_3$, Fucoidan, and FucCeNCs. (i–k) SOD-like activity (i), $^{\bullet}OH$ scavenging ability (j), and DPPH$^{\bullet}$ elimination capacity (k) of FucCeNCs at various concentrations. a.u., arbitrary units. Data are presented as means ± SD (n = 3).

targeting and accumulation of FucCeNCs in sites of colon inflammation.

Afterward, we investigated whether FucCeNCs possess RNOS scavenging activities. First, the SOD-like activity was monitored by monitoring the $O_2^{\bullet-}$ scavenging efficiency. As shown in Figure 3h,i, FucCeNCs demonstrated markedly enhanced SOD-like activity compared with $Ce(NO_3)_3$ or Fucoidan alone, and exhibited a concentration-dependent SOD-like activity. Furthermore, the scavenging abilities of FucCeNCs against hydroxyl radical ($^{\bullet}OH$) and 1,1-Diphenyl-2-picrylhydrazyl radical (DPPH$^{\bullet}$) (a representative RNS species) were examined. Consistently, compared with $Ce(NO_3)_3$ or Fucoidan alone, FucCeNCs showed the strongest scavenging capacity against both radicals (Figure S9a,b) in a concentration-dependent manner (Figure 3j,k). Wherein, the reduction in $^{\bullet}OH$ signal intensity observed via electron paramagnetic resonance (EPR) spectroscopy also verified the direct $^{\bullet}OH$ scavenging ability of FucCeNCs (Figure S10). Notably, $Ce(NO_3)_3$ and Fucoidan alone also showed moderate $^{\bullet}OH$ scavenging ability and DPPH$^{\bullet}$ elimination capacity (Figure S9 and associated discussion).

2.3 | In Vitro Anti-Inflammatory Abilities of FucCeNCs

Upon the onset of IBD, the RNOS increased within colonic lesions is linked to a cascade of inflammatory responses, which may, in turn, contribute to mental disorders through gut–brain axis [7, 10]. Therefore, after evaluation of the RNOS scavenging activities of FucCeNCs, we next explored their anti-inflammatory abilities. We first investigated the cytocompatibility of the FucCeNCs. As depicted in Figure S11, FucCeNCs exhibited negligible cytotoxicity toward RAW264.7 cells even up to 128 μg/mL. Furthermore, hemolytic experiment was conducted using murine erythrocytes. Blood samples were incubated with FucCeNCs at various concentrations and the results demonstrated FucCeNCs are non-hemolytic (Figure S12).

15214095, 0, Downloaded from https://advanced.onlinelibrary.wiley.com/doi/10.1002/adma.202522010 by Nanjing University, Wiley Online Library on [13/02/2026]. See the Terms and Conditions (https://onlinelibrary.wiley.com/terms-and-conditions) on Wiley Online Library for rules of use; OA articles are governed by the applicable Creative Commons License

Subsequently, we evaluated the cytoprotective effect of FucCeNCs in H_2O_2-treated RAW264.7 cells. The results showed that cell viability exhibited a concentration-dependent decrease after incubation with various concentrations of H_2O_2. For example, at 400 μM H_2O_2, cell viability remained approximately 40% (Figure S13), while FucCeNCs alleviated oxidative stress-induced cell death (Figure S14) in a concentration-dependent manner, restoring cell viability to nearly 100%. Since H_2O_2 treatment triggered excessive ROS production, which disrupted mitochondrial homeostasis and ultimately led to cell death, we examined the intracellular ROS scavenging capacity of FucCeNCs using 2′,7′-dichlorofluorescein diacetate (DCFH-DA) as a fluorescent probe. The observation of fluorescence microscope confirmed FucCeNCs treatment presented less DCFH-DA fluorescence intensity in cells compared with other treatments (Figure 4a,b), indicating their effective scavenging of excess ROS induced by H_2O_2. To investigate the effect of FucCeNCs on mitochondrial function, changes in mitochondrial membrane potential were assessed using the fluorescent probe JC-1 (5,5′,6,6′-tetrachloro-1,1′,3,3′-tetraethylbenzimidazolylcarbocyanine iodide). As a key indicator of mitochondrial integrity, mitochondrial membrane potential plays a critical role in ATP synthesis, apoptosis regulation, and antioxidant capacity [41]. Under physiological conditions, JC-1 accumulated in the mitochondrial matrix and forms red fluorescent aggregates. Nevertheless, upon the collapse of the mitochondrial membrane potential, JC-1 dispersed into the cytoplasm as green fluorescent monomers. JC-1 staining analysis revealed that FucCeNCs effectively preserved mitochondrial membrane potential under H_2O_2-induced oxidative stress (Figure S15). Additionally, the protective effect of FucCeNCs against H_2O_2-induced cellular damage was detected using Calcein-AM (green fluorescent dye for live cells) and propidium iodide (PI, red fluorescent dye for dead cells). As shown in Figure S16, the confocal fluorescence images showed that FucCeNCs effectively attenuated H_2O_2-induced cell death in RAW264.7 macrophages, demonstrating their potent cytoprotective effects under oxidative stress conditions. Concurrently, cellular apoptosis was also investigated using Annexin V-FITC/PI staining followed by flow cytometry. The results indicated that H_2O_2 treatment promoted apoptosis, whereas FucCeNCs pretreatment markedly reduced this effect, suggesting a protective role against oxidative damage-induced apoptosis (Figure 4c,d). Given that oxidative damage can exacerbate lipid peroxidation and attenuate the endogenous antioxidant defense system [42], we next evaluated the effects of FucCeNCs on the levels of malondialdehyde (MDA), SOD, and glutathione (GSH). As shown in Figure 4e–g, FucCeNCs treatment significantly decreased MDA content, while increased the levels of SOD and GSH in H_2O_2-treated cells. Thus, the above results indicated FucCeNCs efficiently protect RAW264.7 cells from H_2O_2-induced oxidative stress.

To elucidate the anti-inflammatory mechanism of FucCeNCs against oxidative stress, we examined their modulation of macrophage polarization. Specifically, M1 macrophages are pro-inflammatory, while M2 macrophages are associated with tissue repair and resolution of inflammation. Moreover, M1 and M2 macrophages are identified by CD86 and CD206 markers, respectively [43]. Lipopolysaccharide (LPS) was used to polarize RAW264.7 macrophages to the M1 phenotype. Compared with the LPS group, cells treated with FucCeNCs exhibited a significant downregulation of the M1 marker CD86 (Figure 4h,i) and an upregulation of the M2 marker CD206 (Figure 4j,k). Accordingly, FucCeNCs treatment reduced the secretion of the pro-inflammatory cytokines IL-1β and TNF-α (Figure 4l,m), while enhancing the production of the anti-inflammatory cytokine IL-10 (Figure 4n). Taken together, the outstanding abilities of FucCeNCs to scavenge RNOS, attenuate intracellular oxidative stress, and modulate the inflammatory cytokine profile would support their potential as a therapeutic agent for colitis-associated mental disorders.

2.4 | In Vivo Anti-Inflammation Therapy and Alleviation Effects on UC-Associated Mental Disorders

On the basis of good targeting ability, cytocompatibility, RNOS scavenging activities, and anti-inflammatory effects of FucCeNCs, in vivo therapeutic efficacy was then investigated for DSS-induced UC. Excellent biocompatibility is essential for advancing oral nanotherapeutics into animal studies. Before assessing the therapeutic efficacy of FucCeNCs in treatment of UC, we systematically evaluated their biosafety, which was conducted in healthy mice following oral administration of FucCeNCs (80 mg/kg) for seven consecutive days. With treatment of FucCeNCs, complete blood count analysis in C57BL/6 mice indicated that the levels of red blood cells (RBC), platelets (PLT), monocytes (MON), white blood cells (WBC), and mean corpuscular volume (MCV) were in normal ranges (Figure S17). Meanwhile, no significant changes in serum levels of creatinine (CREA), alanine transaminase (ALT), blood urea nitrogen (BUN), aspartate transaminase (AST), and alkaline phosphatase (ALP) were found after the injection of FucCeNCs (Figure S18). Additionally, Hematoxylin and Eosin (H&E)-stained histological analysis showed that the main organs (heart, liver, spleen, lung, and kidney) were not affected in the FucCeNCs group (Figure S19). These findings demonstrated the excellent biosafety profile of FucCeNCs, suggesting considerable potential for their development as UC-targeted therapeutics.

With a promising biosafety profile established, we therefore assessed the anti-inflammation therapy of FucCeNCs in a murine model of UC. Figure 5a illustrates the overall experimental procedure. DSS-induced UC model was established in mice via ad libitum administration of 3% (w/v) DSS solution for 7 consecutive days. After that, FucCeNCs were administered by oral gavage from the onset of DSS induction. First, we determined the optimal therapeutic dose, DSS-challenged mice were administered with FucCeNCs at 40, 80, and 160 mg/kg doses, respectively. As shown in Figure S20, colon length, a key indicator of UC progression, exhibited a dose-responsive recovery pattern, with maximal restoration achieved at 40 mg/kg compared to DSS group. This dose-dependent response established 40 mg/kg as the optimum, providing the best compromise between efficacy and biosafety (Figures S17–S19). Next, we systematically elucidated the anti-inflammation efficacy of FucCeNCs to UC amelioration through comparative analysis against individual constituents ($Ce(NO_3)_3$ and Fucoidan). The therapeutic doses of $Ce(NO_3)_3$ and Fucoidan were normalized to their constituent concentrations in FucCeNCs to ensure compositional parity across experimental groups. As shown in Figure S21a and S22, control mice without DSS exposure maintained normal behavioral parameters and stable body weight, while DSS-induced UC mice displayed

15214095, 0, Downloaded from https://advanced.onlinelibrary.wiley.com/doi/10.1002/adma.202532010 by Nanjing University, Wiley Online Library on [13/02/2026]. See the Terms and Conditions (https://onlinelibrary.wiley.com/terms-and-conditions) on Wiley Online Library for rules of use; OA articles are governed by the applicable Creative Commons License

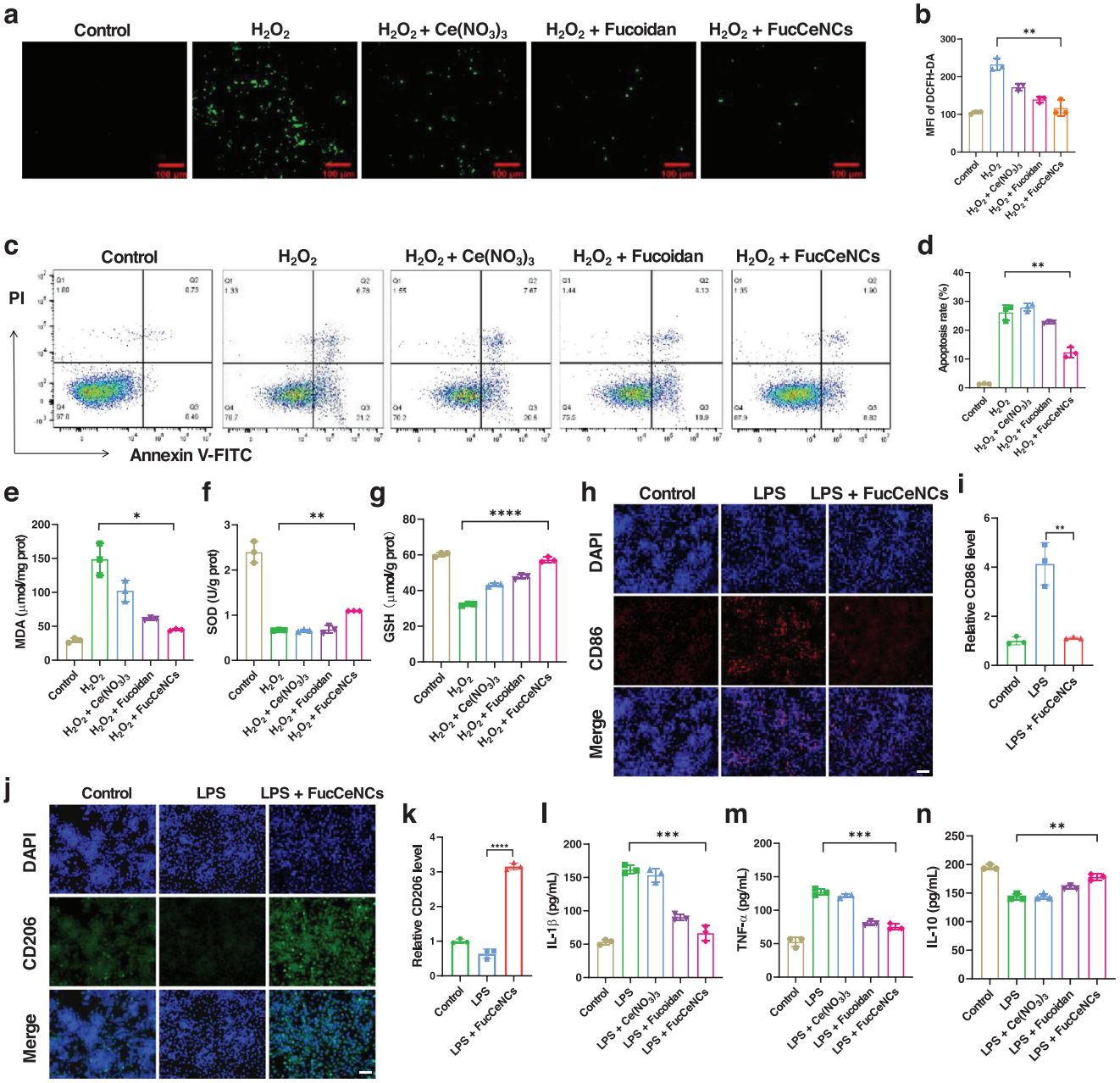

FIGURE 4 | In vitro anti-inflammatory abilities of FucCeNCs. (a,b) Fluorescence microscopy images (a) and quantitative analysis of the average optical density (b) of ROS levels in RAW264.7 cells under H_2O_2 induction. (c,d) Viability (c) and apoptosis (d) of RAW264.7 cells exposed to H_2O_2 were assessed by flow cytometry. (e–g) MDA, SOD, and GSH activities in supernatant after incubation of RAW264.7 cells, respectively. The concentration of H_2O_2 was 400 μM. (h,i) Immunofluorescence images (h) and the corresponding quantification of fluorescence intensity of CD86 (i) in the LPS-induced polarization model of RAW264.7 cells after FucCeNCs treatment. (j,k) Immunofluorescence images (j) and the corresponding quantification of fluorescence intensity of CD206 (k) in the LPS-induced polarization model of RAW264.7 cells after FucCeNCs treatment. (l–n) IL-1β (l), TNF-α (m), and IL-10 (n) levels in LPS-induced RAW264.7 cells from indicated groups. The concentration of LPS was 1 μg/mL. Data are presented as means ± SD (n = 3). Scale bar, 50 μm.

progressive weight loss (retaining 84.93% of baseline) with hallmark symptoms including liquid stool and hematochezia. In contrast, FucCeNCs treatment attenuated disease progression, improving body weight retention to 93.34% of baseline and resolving diarrheal phenotypes. The disease activity index (DAI), a validated clinical scoring system integrating stool consistency, occult blood, and weight loss, objectively quantifies UC progression and therapeutic responses. As demonstrated in Figure S21b, the day-7 DAI scores escalated from 0.17 (healthy group) to 2.56 (DSS group), with partial reduction in $Ce(NO_3)_3$ (2.44) and Fucoidan (1.73) groups. Remarkably, FucCeNCs treatment yielded the lowest DAI (0.81), closely matching the positive control Mesalazine (a clinical reference drug, 0.97), with approaching near-normal clinical parameters. This hierarchy (FucCeNCs < Fucoidan < $Ce(NO_3)_3$< DSS) highlighted the critical role of component synergy in UC mitigation, with FucCeNCs exhibiting superior efficacy compared to individual constituents. Colon morphological analysis further confirmed therapeutic efficacy.

15214095, 0, Downloaded from https://advanced.onlinelibrary.wiley.com/doi/10.1002/adma.202522010 by Nanjing University, Wiley Online Library on [13/02/2026]. See the Terms and Conditions (https://onlinelibrary.wiley.com/terms-and-conditions) on Wiley Online Library for rules of use; OA articles are governed by the applicable Creative Commons License

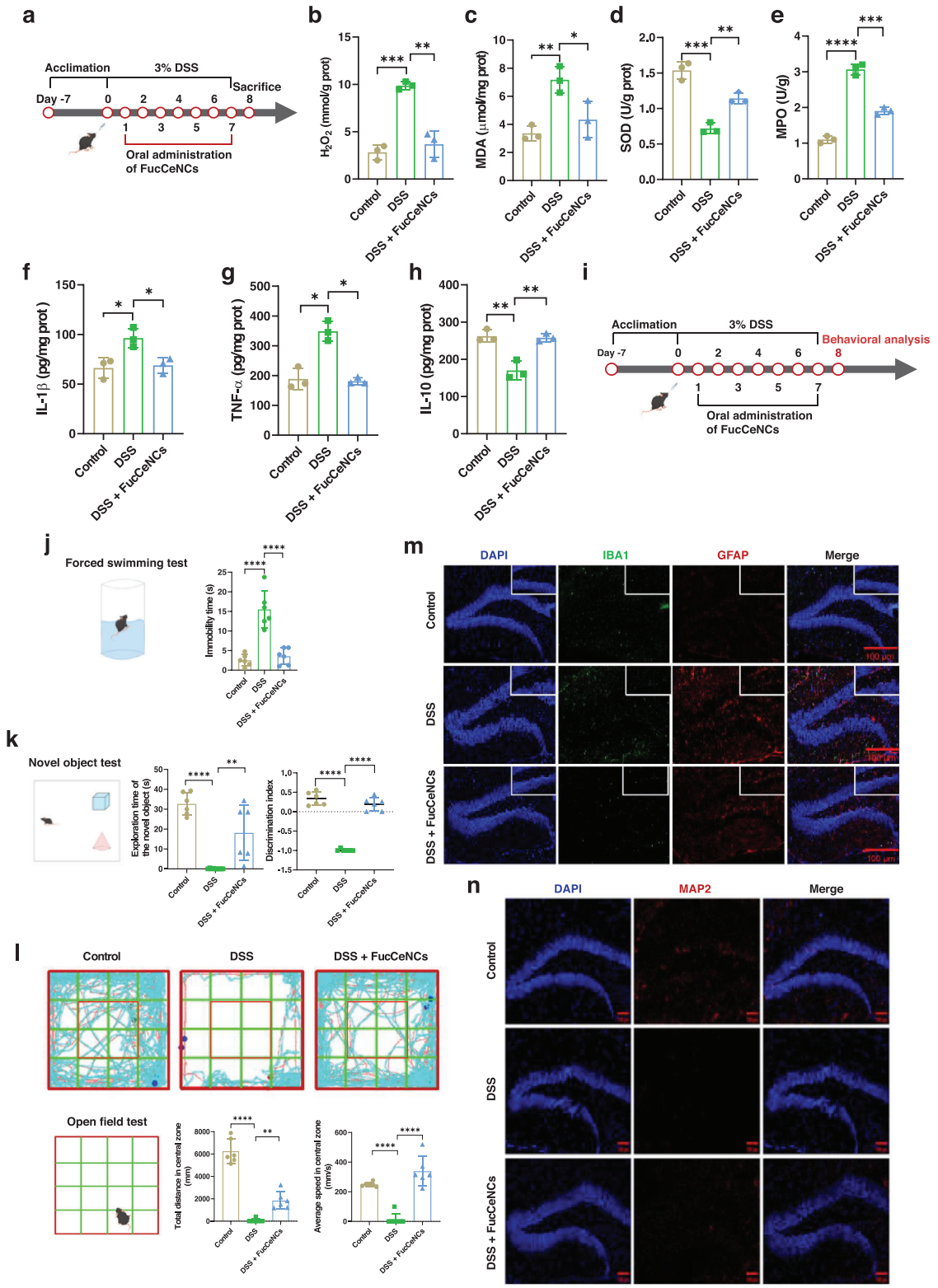

FIGURE 5 | Alleviation effects of FucCeNCs on UC-associated mental disorders. (a) Schematic of experimental timeline in DSS-induced UC. (b–e) Levels of H_2O_2 (b), MDA (c), antioxidant enzymes (SOD and MPO) (d,e) in supernatant after homogenization of colon tissues in different groups (n = 3). (f–h) IL-1β (f), TNF-α (g), and IL-10 (h) levels in colon samples following treatment of FucCeNCs (n = 3). Scale bar, 50 μm. (i) Experimental timeline of behavioral analysis in DSS-induced UC. (j) FST and histogram showing the immobility time of the mice after FucCeNCs treatment (n = 6). (k) NOT and histogram showing the exploration time and discrimination index of the mice following treatment of FucCeNCs (n = 6). (l) OFT (left panel), action roadmap results (top right panel), and histogram showing total distance and average speed (bottom right) of the mice treated with FucCeNCs (n = 6). (m) Immunofluorescence staining results of microglia (IBA1, green) and astrocyte (GFAP, red) in the hippocampi of mice after FucCeNCs treatment. (n) Immunofluorescence staining results of mature neurons (MAP2, red) in the hippocampi of the mice treated with FucCeNCs. Scale bar, 100 μm. Data are presented as means ± SD.

15214095, 0, Downloaded from https://advanced.onlinelibrary.wiley.com/doi/10.1002/adma.202532010 by Nanjing University, Wiley Online Library on [13/02/2026]. See the Terms and Conditions (https://onlinelibrary.wiley.com/terms-and-conditions) on Wiley Online Library for rules of use; OA articles are governed by the applicable Creative Commons License

As shown in Figure S23a,b, FucCeNCs restored colon length from 6.80 ± 0.22 cm (DSS group) to 8.92 ± 0.53 cm (DSS + FucCeNCs group), representing a 31.2% recovery. Importantly, FucCeNCs exhibited comparable therapeutic efficacy to Mesalazine at equimolar doses (40 mg/kg), achieving statistically equivalent colon length restoration (8.92 ± 0.53 cm vs. 8.54 ± 1.37 cm). Furthermore, histopathological analyses confirmed markedly enhanced efficacy of FucCeNCs against DSS-induced pathologies, including colonic mucosal ulceration, crypt distortion, and leukocyte infiltration, relative to $Ce(NO_3)_3$ or Fucoidan treatment (Figure S24), corroborating functional synergy within FucCeNCs in restoring gut homeostasis.

Oxidative stress is a central pathological driver in UC, primarily through RNOS-mediated cellular damage [7]. As demonstrated in Figure 5b, DSS-induced UC triggered a 3.5-fold increase in colonic H_2O_2 levels compared to control group. Treatment with FucCeNCs significantly attenuated this oxidative burst, reducing H_2O_2 production by 63%. Furthermore, FucCeNCs administration decreased MDA, from 7.3 ± 0.9 μmol/mg prot (DSS group) to 4.3 ± 1.3 μmol/mg prot, indicating mitigation of oxidative membrane damage (Figure 5c). Concurrently, the compromised activities of key antioxidant enzymes, SOD and myeloperoxidase (MPO), were restored after FucCeNCs treatment (Figure 5d,e). The colonic epithelial barrier, key guardian of gut homeostasis, suffers oxidative disruption from pathologically amplified RNOS fluxes in UC, where excessive $O_2^{\bullet-}/H_2O_2$ directly compromise tight junction integrity through lipid peroxidation and Occludin/ZO-1 oxidation [44]. Immunofluorescence imaging demonstrated that Occludin and ZO-1 displayed uniform distribution in control group, consistent with intact tight junction architecture. However, DSS-induced injury triggered pronounced redistribution of both proteins, characterized by fragmented signal patterns and diminished intensity, indicative of paracellular barrier compromise. FucCeNCs administration reversed DSS-induced Occludin/ZO-1 dislocation, mechanistically underpinning barrier protection via RNOS neutralization and tight junction restitution (Figures S25 and S26); orthogonal validation through fluorescence intensity quantification in Figure S27a,b corroborated this functional rescue. In addition, FucCeNCs enhanced mucopolysaccharide production and maintained mucus barrier function, as evidenced by Periodic Acid-Schiff (PAS) staining of goblet cells (Figure S28). Thus, FucCeNCs scavenged lumenal RNOS to safeguard tight junction plasticity.

Afterward, we evaluated the effects of FucCeNCs on inflammatory responses in DSS-induced UC. As quantified in Figure 5f,g, DSS exposure provoked a robust systemic inflammatory response, elevating colonic IL-1β concentrations from 66.3 ± 10.1 pg/mg prot (control) to 96.4 ± 9.7 pg/mg prot (DSS group), and TNF-α levels from 188.8 ± 36.4 pg/mg prot (control) to 348.8 ± 33.9 pg/mg prot (DSS group). Notably, FucCeNCs supplementation effectively suppressed this upregulation, attenuating DSS-driven inflammatory cascade. Conversely, DSS treatment reduced the expression of anti-inflammatory cytokine IL-10, while FucCeNCs administration restored IL-10 levels to near-normal values (Figure 5h). Moreover, DSS challenge triggered pronounced splenomegaly, a hallmark of systemic inflammation, which was significantly attenuated with FucCeNCs treatment through reduction of splenic hypertrophy (Figure S29a). Consistent with macroscopic observations, quantitative analysis of the spleen organ index (spleen weight/body weight) revealed that DSS administration elevated this parameter from 3.8 ± 0.7 mg/g in controls to 9.1 ± 1.2 mg/g (DSS group), while FucCeNCs intervention restored the index to 5.8 ± 1.1 mg/g, demonstrating therapeutic efficacy in reversing pathological splenic remodeling (Figure S29b). Collectively, these findings demonstrated that FucCeNCs ameliorated experimental UC through mitigation of oxidative stress and suppression of inflammatory cascades, leading to restoration of colonic mucosal integrity and mitigation of systemic inflammation.

Emerging evidence implicates pro-inflammatory cytokines and gut barrier impairment in transmitting inflammatory signals to the central nervous system through vagus nerve or systemic circulation via gut–brain axis, thereby driving depression-/anxiety-like behavior [15, 45, 46]. Given the anti-inflammatory and gut barrier-protective effects of FucCeNCs in DSS-induced UC mice, we further evaluated its capacity to alleviate UC-associated neuropsychiatric comorbidities. Behavioral assays (forced swimming test (FST), novel object test (NOT), and open field test (OFT)) were performed in DSS-induced UC mice (Figure 5i). In the FST (Figure 5j), mice in DSS-induced group exhibited prolonged immobility (15.5 ± 4.8 s vs. control 2.5 ± 1.5 s), reversed by FucCeNCs (3.5 ± 2.1 s). NOT showed that mice reduced novel object exploration time (DSS 32.6 ± 5.7 s vs. control 0.1 ± 0.2 s) and discrimination index (DSS 0.18 ± 0.05 vs. control 0.52 ± 0.07) in DSS-induced group, both rescued after FucCeNCs treatment (exploration: 59 ± 5%; discrimination: 0.43 ± 0.06) (Figure 5k; Figure S30). OFT analyses revealed that DSS-induced mice exhibited wall-hugging behavior with minimal central exploration, whereas FucCeNCs treatment restored central exploration and increased total movement distance, indicating amelioration of psychomotor retardation and cognitive decline (Figure 5l). Notably, while some mitigation of weight loss (Figure S21a) and DAI (Figure S21b) was observed after FucCeNCs treatment, these physical parameters remained notably distinct from healthy controls. These results indicated that the antidepressant effect of FucCeNCs was not solely dependent on general physical recovery.

Immunofluorescence staining of brain tissues further validated these findings. Ionized calcium-binding adapter molecule 1 (IBA1)/glial fibrillary acidic protein (GFAP) staining revealed microglial/astrocyte hyperactivation (enhanced fluorescence) in DSS-induced UC mice, normalized by FucCeNCs (Figure 5m; Figure S31a,b). Microtubule-associated protein 2 (MAP2) staining showed reduced fluorescence intensity in the hippocampus of DSS-induced colitis mice (decreased fluorescence intensity), which was restored following FucCeNCs treatment (Figure 5n; Figure S31c). Combined with behavioral data, these results demonstrated FucCeNCs' dual neuroprotective mechanisms: (1) suppressing microglial/astrocyte overactivation to attenuate neuroinflammation, and (2) preserving MAP2 expression to restore neuronal structural integrity. This synergistic action provided critical evidence that gut inflammation was key target for Fucoidan in the treatment of colitis-associated mental disorders via gut–brain axis in Figure 2.

15214095, 0, Downloaded from https://advanced.onlinelibrary.wiley.com/doi/10.1002/adma.202522010 by Nanjing University, Wiley Online Library on [13/02/2026]. See the Terms and Conditions (https://onlinelibrary.wiley.com/terms-and-conditions) on Wiley Online Library for rules of use; OA articles are governed by the applicable Creative Commons License

2.5 | Modulation of the Gut Microbiota and Its Derived Bioactive Metabolites of FucCeNCs

In addition to inflammation, UC is also associated with gut microbiota dysbiosis, which in turn can influence brain function and behavior via the bidirectional signaling of microbiota-gut–brain axis [9, 14]. Importantly, polysaccharides serve as prebiotics to regulate the composition of gut microbiota and stimulate the production of beneficial microbial metabolites to attenuate neuroinflammation via the microbiota-gut-brain axis [29]. Building upon this, we further investigated the therapeutic potential of FucCeNCs in restoring gut microbiota homeostasis by 16S ribosomal RNA gene sequencing. α-diversity analysis was performed using the Chao (species richness), Shannon (community diversity), and Simpson (dominance structure) indices. As demonstrated in Figure 6a–c, DSS-induced colitis mice displayed marked microbial community collapse relative to controls, evidenced by significant reductions in Chao and Shannon indices, with a concomitant increase in Simpson index. These alterations cumulatively delineated a characteristic depletion of gut microbial species richness and α-diversity indices in DSS-induced UC murine models. Conversely, treatment with FucCeNCs resulted in a significant restoration of gut microbial diversity, as indicated by an increase in the Chao and Shannon indices and a decrease in the Simpson index to levels comparable to healthy controls. This confirmed the efficacy of FucCeNCs in modulating core α-diversity parameters under pathological conditions. Then, multivariate β-diversity analysis via Bray-Curtis-based Principal Coordinates Analysis (PCoA) revealed significant intergroup segregation along principal coordinates (PC1: 40.73%; PC2: 22.57%), and FucCeNCs group showed a significant difference compared to that of the DSS group and closer to that of the healthy controls (Figure 6d). These results demonstrated FucCeNCs-driven amelioration of UC-associated dysbiotic configuration through ecological restructuring diverging from disease-associated community archetypes.

To systematically evaluate FucCeNCs treatment on gut microbial community structure, we conducted a multi-level taxonomic analysis by constructing relative abundance distribution bar plots at phylum, family, and genus levels. As shown in Figure 6e, the phylum-level profiling revealed that the control (healthy) group's microbiota was predominantly composed of *Bacillota*, *Bacteroidota*, *Campylobacterota*, *Pseudomonadota*, and *Verrucomicrobiota*, with the top three dominant phyla (*Bacillota*, *Bacteroidota*, and *Campylobacterota*) accounting for 95% cumulative relative abundance. Compared to controls, the DSS-induced model group exhibited significantly decreased *Bacillota* abundance alongside significant enrichment of *Campylobacterota* and *Pseudomonadota*, a pattern consistent with prior UC model studies [9]. FucCeNCs intervention restored *Bacillota* abundance to control-equivalent levels while reducing *Campylobacterota* and *Pseudomonadota* proportions relative to the DSS-induced group. At the family taxonomic level, significant compositional disparities were observed among the three experimental groups (Figure 6f). Specifically, the DSS-induced model group exhibited significant proliferation of *Helicobacteraceae* and *Enterobacteriaceae* (Figure 6g,h), while demonstrating reduced relative abundance of *Lactobacillaceae* and *Muribaculaceae* (Figure 6i,j). Following FucCeNCs treatment, the relative abundance of *Lactobacillaceae* and *Muribaculaceae* was significantly restored, with concurrent suppression of *Helicobacteraceae* and *Enterobacteriaceae* proportions. Additionally, Genus-level taxonomic analysis revealed significant intergroup divergence in gut microbiota composition (Figure S32). Compared to the control group, the DSS-induced UC model exhibited statistically significant reductions in symbiotic genera *Clostridium* and *Muribaculum*, concurrently demonstrating marked enrichment of conditionally pathogenic genera *Helicobacter* and *Escherichia*. After FucCeNCs treatment, DSS-triggered dysbiosis showed notable amelioration, characterized by restorative trends in *Clostridium* and *Muribaculum* relative abundance [47]. Subsequently, linear discriminant analysis (LDA) Effect Size (LEfSe) was also carried out to identify the specialized microbial communities between FucCeNCs treatment and the DSS-induced group. We identified 18 differentially abundant taxa. As shown in Figure 6k,l, the DSS group was enriched with *Gammaproteobacteria*, *Enterobacteriaceae*, and *Escherichia* (conditional pathogens), while the FucCeNCs group showed increased abundance of anti-inflammatory commensals such as *Clostridia* and *Muribaculaceae* [48]. These findings suggested that FucCeNCs critically regulated gut ecosystem homeostasis by targeting keystone bacterial equilibria.

Previous research has demonstrated that bioactive metabolites derived from the gut microbiota enter the systemic circulation, where they could traverse or modulate the blood-brain barrier (BBB), thereby regulating brain function to reduce neuroinflammation [13, 14, 49]. Following the demonstrated efficacy of FucCeNCs treatment in gut microbiome amelioration, we next investigated another possible action mechanism of alleviation effects on UC-associated depressive and anxious behaviors via untargeted metabolomic analysis of fecal metabolites. First, principal component analysis (PCA) demonstrated a distinct separation among the healthy (termed as Control), DSS-treated, and DSS + FucCeNCs-treated mice (Figures S33a and S34a). Volcano plot analysis identified 1229 DEGs between the Control and DSS groups, of which 914 were up-regulated and 315 were down-regulated. Following FucCeNCs treatment, 117 genes were significantly altered compared to the DSS group alone, comprising 95 up-regulated and 22 down-regulated genes. These results indicated FucCeNCs markedly modulated the expression of genes associated with fecal metabolite profiles in DSS-induced UC (Figures S33b and S34b). To explore the biological functions of these genes, we then conducted a KEGG functional enrichment analysis. The results demonstrated that, in comparison with the DSS group, FucCeNCs treatment significantly modulated a variety of metabolic pathways, encompassing amino acid biosynthesis/metabolism, lipid metabolism, carbohydrate metabolism, and the metabolism of cofactors and vitamins (Figure 7a; Figure S35a). Importantly, the abnormal biosynthesis and metabolism of amino acids were markedly attenuated (Figure 7b; Figure S35b). Moreover, these alterations were associated with the biosynthetic pathways of valine, leucine (and isoleucine), phenylalanine, tyrosine, and tryptophan (Figure 7c; Figure S35c). Of particular significance was the pronounced reduction in the levels of valine, leucine/isoleucine, phenylalanine, and tryptophan (Figure 7d–g),

15214095, 0, Downloaded from https://advanced.onlinelibrary.wiley.com/doi/10.1002/adma.202532010 by Nanjing University, Wiley Online Library on [13/02/2026]. See the Terms and Conditions (https://onlinelibrary.wiley.com/terms-and-conditions) on Wiley Online Library for rules of use; OA articles are governed by the applicable Creative Commons License

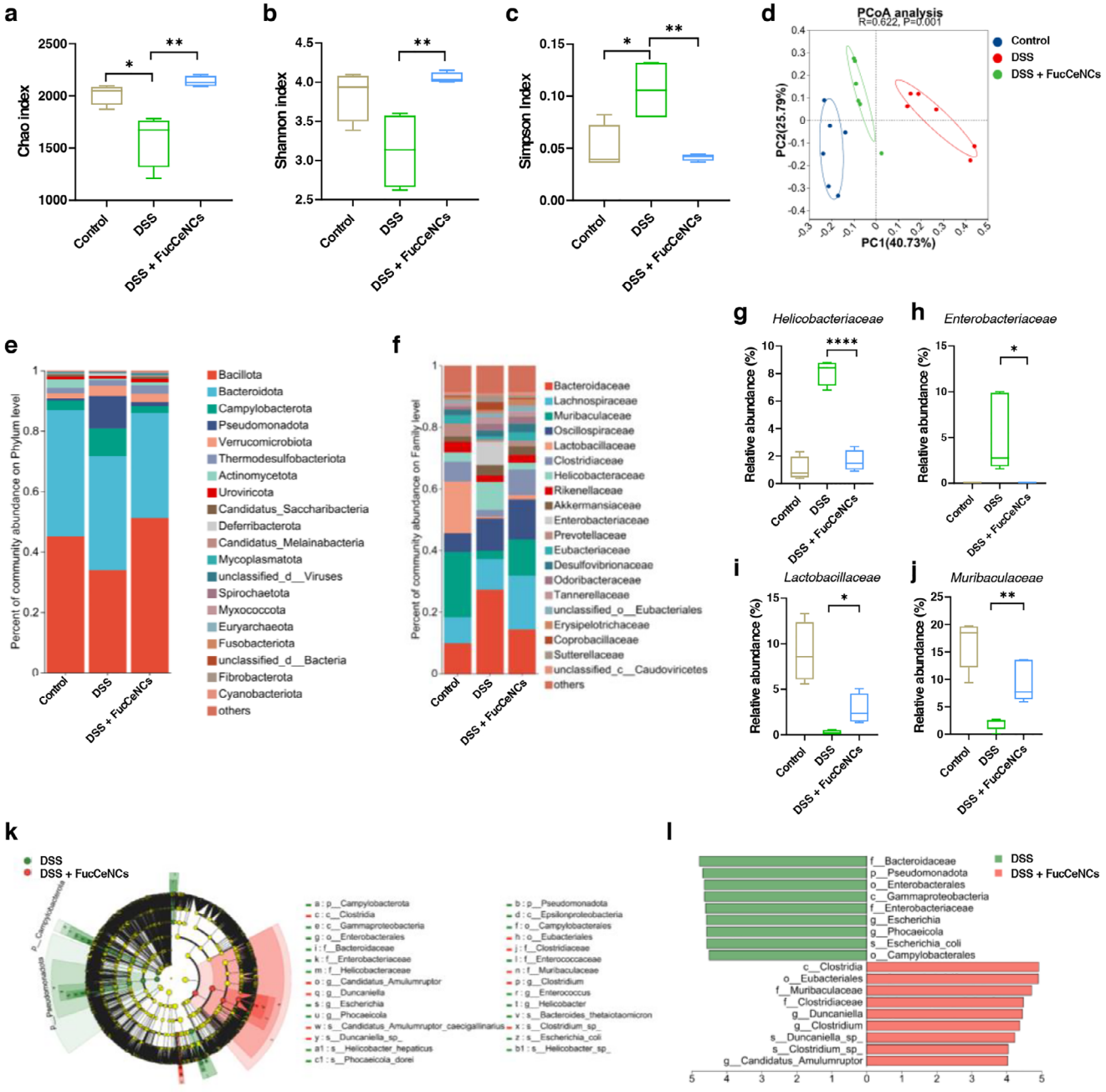

FIGURE 6 | Gut microbiome amelioration in mice with DSS-induced UC after FucCeNCs treatment. (a–c) Chao (a), Shannon, (b) and Simpson (c) indices of gut microbiome from healthy group (Control), DSS-treated group (DSS), and DSS + FucCeNCs-treated group. (d) PCoA analysis of transcriptome profiles. (e,f) Relative abundance histogram of gut microbiota at phylum (e) and family (f) levels. (g–j) Relative abundance of family-level taxa for *Helicobacteriaceae* (g), *Enterobacteriaceae* (h), *Lactobacillaceae* (i), and *Muribaculaceae* (j), respectively. (k) Cladogram of LEfSe analysis illustrating the community composition of gut microbiota of the mice treated with or without FucCeNCs. Green and red circles represent the enriched taxa in the DSS and FucCeNCs-treated groups, respectively; Yellow circles represent the detected but not enriched taxa. (l) LDA showing the significantly enriched taxa between DSS and FucCeNCs-treated groups. Data are presented as means ± SD (n = 5).

which are conducive to regulate gut homeostasis and the immune system, alleviating inflammation [50, 51].

Furthermore, the final metabolite of phenylalanine, homovanillic acid (HVA), significantly increased after treatment with FucCeNCs (Figure 7h). Mechanistically, HVA mediates neuroprotection through suppression of excessive autophagy in hippocampal neurons and upregulation of the presynaptic protein synapsin 1 (SYN1), thereby preserving neuronal integrity and synaptic ultrastructure [52]. To determine whether HVA inhibits autophagy and protects synapses, we performed Western blot analysis in glucose-deprived HT22 mouse neuronal cells. As shown in Figure S36, glucose deprivation (a stimulus mimicking nutrient starvation) activated autophagy, evidenced by increased LC3I to LC3II conversion and a higher LC3-II/LC3-I ratio. HVA treatment reversed this increase, indicating potent autophagy inhibition.

15214095, 0, Downloaded from https://advanced.onlinelibrary.wiley.com/doi/10.1002/adma.202522010 by Nanjing University, Wiley Online Library on [13/02/2026]. See the Terms and Conditions (https://onlinelibrary.wiley.com/terms-and-conditions) on Wiley Online Library for rules of use; OA articles are governed by the applicable Creative Commons License

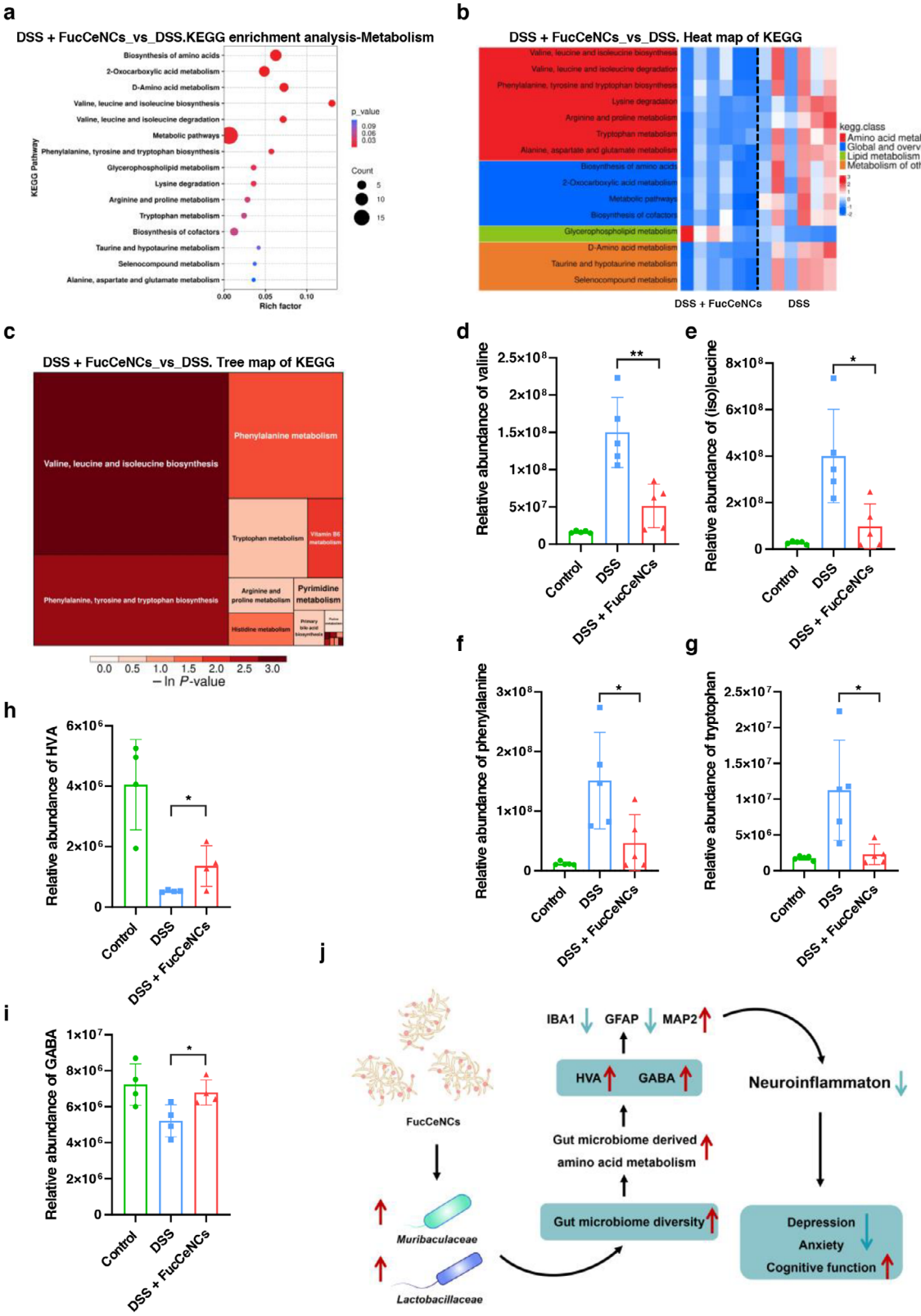

FIGURE 7 | Gut microbiota-derived bioactive metabolites in alleviating UC-related depression and anxiety after FucCeNCs treatment. (a) Functional enrichment analysis of gut microbiome metabolites via KEGG pathway. (b,c) A heat map for each mouse (column) (b) and tree map (c) of significant changes in gut microbiome metabolites. (d–g) Relative abundance of valine (d), (iso)leucine (e), phenylalanine (f), and tryptophan (g), respectively (n = 5). (h,i) Relative abundance of amino acid metabolites in the feces of mice for HVA (h) and GABA (i), respectively (n = 4). (j) Proposed pathway of FucCeNCs in inhibiting neuroinflammation through regulating gut microbiome metabolites. Data are presented as means ± SD.

15214095, 0, Downloaded from https://advanced.onlinelibrary.wiley.com/doi/10.1002/adma.202522010 by Nanjing University, Wiley Online Library on [13/02/2026]. See the Terms and Conditions (https://onlinelibrary.wiley.com/terms-and-conditions) on Wiley Online Library for rules of use; OA articles are governed by the applicable Creative Commons License

Furthermore, HVA rescued the expression of SYN1, which was downregulated under glucose deprivation and linked to synaptic impairment, thereby exhibiting a synaptic protective effect. Additionally, FucCeNCs treatment markedly reduced the relative abundance of γ-aminobutyric acid (GABA), a neurotransmitter that can cross the BBB or signal via vagus nerve, attenuating neuroinflammation and mitigating mental disorders (Figure 7i) [44, 53].

Having established that gut microbiota could produce HVA and GABA (Figure 7h,i), we next evaluated whether these metabolites could access the brain via the microbiota-gut-brain axis. The results revealed that FucCeNCs treatment markedly elevated the brain levels of both HVA (Figure S37a) and GABA (Figure S37b). Together, the above results indicated that FucCeNCs alleviate UC-associated depression- and anxiety-like behaviors by restoring gut microbial homeostasis, thereby facilitating the production of bioactive amino acid metabolites, which enhanced neuronal repair and attenuate neuroinflammation (Figure 7j). Thus, inconsistent with the metabolic pathways predicted in Figure 2, gut microbiota-derived amino acid metabolism, especially bioactive metabolites, was identified as another pivotal therapeutic target for colitis-associated mental disorders via microbiome-gut–brain axis.

Maintaining the gastrointestinal stability of orally administered FucCeNCs is crucial for therapeutic efficacy. To evaluate this, we assessed the structural integrity of FucCeNCs by measuring Ce release in simulated gastric fluid (SGF, pH = 2) and simulated intestinal fluid (SIF, pH = 6.8). As shown in Figure S38, 50% Ce retention in SGF and 80% in SIF, indicating about ~50 % of FucCeNCs resisted gastric degradation to reach the colon. To overcome this limitation, we employed enteric-coated capsules for the oral administration of FucCeNCs (designated as Capsules). Comparison of colon lengths in UC mice demonstrated the considerable therapeutic efficacy of the treatment of Capsules (Figure S39). This pharmaceutically viable strategy enabled site-specific release into the colon, thereby improving therapeutic precision and offering a scalable platform for future clinical application in UC-associated mental disorders.

3 | Conclusion

In summary, guided by bioinformatic prediction of Fucoidan's potential targets, oral polysaccharide engineered nanozymes, FucCeNCs with anti-inflammatory and gut microbiota-derived metabolism regulating activities were developed to treat UC-associated mental disorders. The designed FucCeNCs were fabricated by chelation-driven assembly of Ce ions with Fucoidan. After oral delivery, FucCeNCs (negative charges) could directly target positively charged inflamed colon through electrostatic interactions. Compared with Ce^{3+} or Fucoidan alone, FucCeNCs exhibited higher RNOS-scavenging capacity, attributable to the reversible Ce^{3+}/Ce^{4+} valence transition. This activity further facilitated the polarization of macrophages from the pro-inflammatory M1 to the anti-inflammatory M2 phenotype, leading to the upregulation of anti-inflammatory cytokines. Through the mitigation of oxidative stress and inflammatory cascades, FucCeNCs restored colonic mucosal integrity and reduced systemic inflammation, thereby suppressing microglial/astrocytic overactivation and preserving neuronal integrity through the transmission of anti-inflammatory cytokines via gut–brain axis. Specially, FucCeNCs enriched gut microbiota diversity, favoring beneficial species and suppressing pathogens. This reconfigured microbiome promoted probiotics to produce bioactive amino acid metabolites, such as HVA and GABA. These metabolites, in turn, suppressed excessive autophagy in hippocampal neurons, promoted neurotransmitter release, attenuated neuroinflammation, and ultimately ameliorated depression- and anxiety-like behaviors via microbiome-gut–brain axis. This work not only establishes a strategy for bioinformatics-guided polysaccharide engineered nanozyme design that transcends small-molecule drugs in treating colitis-associated mental disorders, but also highlights gut inflammation and gut microbiota-derived metabolism, especially bioactive metabolites as key targets via microbiota-gut–brain axis, offering a promising strategy for IBD treatment and its comorbidities.

4 | Experimental Methods

4.1 | Synthesis and Purification of FucCeNCs

FucCeNCs were synthesized and purified as follows. First, Fucoidan (100 mg) and $Ce(NO_3)_3{\cdot}6H_2O$ (2 M) were dissolved in ultrapure water under constant stirring. The pH of the reaction mixture was adjusted to 8–9 with 2 M NaOH and maintained at 70°C for 60 min. Then, the crude product was initially purified by centrifugation at 8000 rpm for 5 min. A three-fold volume of anhydrous ethanol was added to the supernatant, and the mixture was centrifuged again (8000 rpm, 5 min). Subsequently, the pellet was resuspended in 3 mL of ultrapure water, and the resulting suspension was dialyzed (MWCO: 3500 Da) against ultrapure water for 24 h to remove free ions. Final purification was achieved through reprecipitation with anhydrous ethanol, centrifugation (8000 rpm, 5 min), and lyophilization, yielding FucCeNCs as a loose powder.

4.2 | Measurement of SOD-Like Activity

The SOD-like activity was investigated by using a SOD assay kit. Initially, 20 μL of FucCeNCs at various concentrations (7.8, 15.6, 31.2, 62.5, and 125.0 μg/mL) was mixed with 200 μL of a 2-(4-iodophenyl)-3-(4-nitrophenyl)-5-(2,4-disulfophenyl)-2H tetrazolium sodium salt working solution. Then, 20 μL of the enzyme working solution was added, and the mixture was incubated at 37°C for 20 min. The absorbance was finally measured at 450 nm using a microplate reader.

4.3 | Measurement of $^{\bullet}OH$ Scavenging Activity

$^{\bullet}OH$ scavenging activity of FucCeNCs was detected in a Fenton reaction system. The generated $^{\bullet}OH$ was trapped in aqueous solution using the spin trap agent DMPO and detected by EPR spectroscopy. In a typical experiment, a glass capillary tube containing FucCeNCs (40 μg/mL), H_2O_2 (1.0 mM), $FeSO_4$ (1.0 mM), DMPO (10 mM), and PBS buffer (0.01 M, pH 7.2) was

15214095, 0, Downloaded from https://advanced.onlinelibrary.wiley.com/doi/10.1002/adma.202522010 by Nanjing University, Wiley Online Library on [13/02/2026]. See the Terms and Conditions (https://onlinelibrary.wiley.com/terms-and-conditions) on Wiley Online Library for rules of use; OA articles are governed by the applicable Creative Commons License

inserted into the EPR cavity to record $^{\bullet}OH$ signals after 5 min of reaction.

4.4 | Measurement of DPPH$^{\bullet}$ Scavenging Activity

The scavenging activity of FucCeNCs against DPPH$^{\bullet}$ was assessed by measuring the decrease in absorbance at 517 nm. A stock solution of DPPH (125 μM) was prepared in anhydrous ethanol and stored in the dark. Equal volumes of above DPPH solution and FucCeNCs at various concentrations (0.02, 0.1, 0.5, 2.0, 4.0, and 8.0 μg/mL) were mixed and incubated at 37°C for 15 min in the dark. The absorbance was then measured by using a microplate reader.

4.5 | In Vitro Cytotoxicity Experiments

RAW264.7 cells were seeded in 96-well plates at a density of 1×10^4 cells per well and cultured for 12 h. The cells were then pretreated for 1 h with (I) PBS (negative control), (II) $Ce(NO_3)_3$ (0.184 μg/mL), (III) Fucoidan (1.04 μg/mL), or (IV) FucCeNCs (4 μg/mL). Subsequently, oxidative stress was induced by adding H_2O_2 (400 μM) for 24 h. Then, the cell viability was measured using MTT assay. Briefly, 10 μL of MTT solution (5 mg/mL) was added to each well and incubated at 37°C for 4 h in the dark. After removing the culture medium, 100 μL of DMSO was added to dissolve the formazan crystals. The absorbance was determined at 570 nm, and the cell viability was expressed as a percentage of the control.

4.6 | Determination of Intracellular ROS

RAW264.7 cells were seeded in 6-well plates at a density of 1×10^5 cells per well and treated with (I)—(IV), followed by H_2O_2 exposure. After treatment, the cells were washed twice with sterile PBS. Then, they were stained with 10 μM DCFH-DA for 30 min in the dark at room temperature. The intracellular ROS levels were measured using a confocal laser microscope with excitation and emission wavelengths at 488 and 525 nm, respectively.

4.7 | Live/Dead Cell Viability and Mitochondrial Membrane Potential Assay

The RAW264.7 cells treated by (I)—(IV) were stained with Calcein-AM (2.5 μM) and PI (5 μg/mL) for 45 min and washed three times with sterile PBS for visualization via a confocal fluorescence microscope. For the measurement of mitochondrial membrane potential, JC-1 staining was performed following the same experimental procedure.

4.8 | In Vivo Biosafety Assessment

All animal experiments were approved by the Committee for Experimental Animals Welfare and Ethics of Yangzhou University (Institutional Animal Care and Use Committee, 202402032). Male C57BL/6 mice (6-8 weeks old) were randomly assigned to two groups (five mice per group): a control group by *i. g.*-delivered PBS and an experimental group by *i. g.* treatment with FucCeNCs. The experimental group received oral administration of FucCeNCs at a daily dose of 80 mg/kg for 7 consecutive days, while the control group was given an equal volume of PBS. After 24 h, blood samples were collected via retro-orbital puncture, and serum was separated for assessment of key biochemical parameters using an automated biochemistry analyzer. At the end of the experiment, all mice were euthanized, and major organs/tissues (heart, liver, spleen, lungs, kidneys, and colons) were systematically harvested. The organs/tissues were fixed in 4% paraformaldehyde, routinely embedded in paraffin, sectioned, and stained with H&E for histopathological analysis to evaluate the potential toxicity of FucCeNCs.

4.9 | Treatment of UC in DSS-Induced Mice

Male C57BL/6 mice (18 to 20 g) were acclimatized for 7 days and randomly divided into various groups with five mice per group. On the eighth day, except for the control group, mice were administered 3% (w/v) DSS solution, which was filter-sterilized through a 0.22 μm membrane, in their drinking water ad libitum for 7 consecutive days to establish a DSS-induced UC model. Note that this day was designated as day 0. DSS-induced UC mice were administered FucCeNCs (40 mg/kg) or Mesalazine (40 mg/kg) on days 1, 3, 5, and 7 by *i. g.* injection. Body weight and DAI were recorded for 8 consecutive days. On day 8, all mice were euthanized, and spleen samples were collected and weighed; colon length was measured. Additionally, colon tissues were subjected to further analyses, including H_2O_2, MDA, antioxidant enzyme activities, inflammatory cytokine levels, as well as H&E staining and immunofluorescence assays.

4.10 | Forced Swimming Test

Following administration of FucCeNCs, FST was conducted in a transparent polycarbonate cylinder (20 cm diameter × 30 cm height) filled with purified water to a depth of 15 cm, maintained at 22–24°C. Each mouse was individually placed into the water and allowed to swim for 6 min. The immobility time during the final 4 min was analyzed using a video tracking system (Supermaze V2.0, Shanghai Xinruan Information Technology Co., Ltd.). Immobility was defined as the absence of active escape-related behaviors, with only minimal movements necessary to maintain the head above the water surface.

4.11 | Novel Object Test

After FucCeNCs treatment, NOT was performed using a standardized two-phase protocol:

1. Habituation phase: Mice were individually placed in an open-field arena containing two identical azure cubes (5 × 5 × 5 cm) and permitted to explore freely for 10 min.
2. Test phase (24 h post-habituation): One familiar object was replaced with a novel pink cone (base diameter: 5 cm; height: 7 cm). Exploratory behavior was video-recorded for

15214095, 0, Downloaded from https://advanced.onlinelibrary.wiley.com/doi/10.1002/adma.202532010 by Nanjing University, Wiley Online Library on [13/02/2026]. See the Terms and Conditions (https://onlinelibrary.wiley.com/terms-and-conditions) on Wiley Online Library for rules of use; OA articles are governed by the applicable Creative Commons License

10 min, and the time spent investigating the novel object was quantified. Investigation was defined as the mouse orienting its snout toward the object within ≤ 2 cm, with clear attention and nose-pointing orientation.

4.12 | Open Field Test

Following treatment with FucCeNCs, OFT was conducted in a custom-built, enclosed, light-attenuated open-field chamber. The floor of the arena was divided into a 4 × 4 grid, with the central zone defined as the eight innermost squares. Before each test session, the apparatus was meticulously cleaned with 75% ethanol to remove residual olfactory cues. Individual mice were placed in the center of the arena and allowed to explore freely for 5 min while being recorded by a video tracking system (Supermaze V2.0, Shanghai Xinruan Information Technology Co., Ltd.). The following behavioral parameters were quantified: time spent in the central zone (s), number of entries into the central zone, and total distance traveled within the central zone (mm).

4.13 | Measurement of GABA and HVA in Brain Tissues

The concentration of GABA in mouse brain tissue was analyzed using a GABA assay kit. Brain tissues from the healthy control, DSS-treated, and DSS + FucCeNCs-treated groups were processed as follows: brain tissue was homogenized in ice-cold physiological saline (0.9% NaCl) at a 1:9 (w/v) ratio. The homogenate was centrifuged at 10 000 × g for 10 min at 4°C, and the supernatant was collected. Then, the supernatant was ultrafiltered using a 3 kDa molecular weight cutoff device by centrifugation at 12,000 × g for 15 min at 4°C. The resulting filtrate was kept on ice for subsequent analysis. Afterward, 20 μL of sample was dispensed into the appropriate microplate wells, followed by 200 μL of working solution. After agitation for 3 s, the plate was incubated at 37°C for 30 min in the dark. Fluorescence was measured using a microplate reader with excitation/emission wavelengths of 535 and 587 nm, respectively. GABA concentrations were final calculated according to the manufacturer's protocol. Similarly, HVA was quantified following the above-described procedure.

4.14 | Western Blotting Assay

HT22 mouse neuronal cells were lysed in ice-cold radioimmunoprecipitation assay (RIPA) buffer containing a protease inhibitor cocktail (phenylmethanesulfonyl fluoride, PMSF), and protein concentrations were determined using a BCA assay kit. Equal amounts of protein lysates were separated by sodium dodecyl sulfate-polyacrylamide gel electrophoresis (SDS-PAGE) and electro-transferred onto polyvinylidene fluoride (PVDF) membranes. After blocking with 5% non-fat milk, the membranes were incubated overnight at 4°C with primary antibodies against LC3B, SYN1, and β-actin. Following washes, membranes were incubated with appropriate horseradish peroxidase (HRP)-conjugated secondary antibodies at room temperature for 1 h. Finally, protein bands were visualized and densitometric analysis was performed with ImageJ v1.54f.

4.15 | Resistance Assay of FucCeNCs In Vitro

FucCeNCs enclosed in dialysis tubing were incubated in SGF/SIF at 37°C for 4 h. Ce content in the release medium collected was quantified by ICP-OES to assess FucCeNCs' stability.

4.16 | Statistical Analysis

Statistical analysis was performed using Student's t test for two-group differences and one-way two-sided analysis of variance (ANOVA) for multiple comparisons by GraphPad Prism 8. *p < 0.05, **p < 0.01, ***p < 0.001, and ****p < 0.0001. The statistical graphs were all presented as mean ± standard deviation (SD). The sample size n was indicated in the figure captions.

Acknowledgements

This work was supported by the National Natural Science Foundation of China (22472146), the Natural Science Foundation of Jiangsu Province (BK20231329), Natural Science Foundation of Jiangsu Higher Education Institution (25KJD416004), Yangzhou "Lvyang Jinfeng" Talent Program (YZLYJFJH2024YXBS164), Yangzhou Key Research, Development Program (Social Development) (YZ2024084), China Postdoctoral Science Foundation (2025M782949), and the Natural Science Foundation of Yangzhou (YZ2025125).

Funding

National Natural Science Foundation of China (22472146), Natural Science Foundation of Jiangsu Province (BK20231329), Natural Science Foundation of Jiangsu Higher Education Institution (25KJD416004), Yangzhou "Lvyang Jinfeng" Talent Program (YZLYJFJH2024YXBS164), Yangzhou Key Research, Development Program (Social Development) (YZ2024084), China Postdoctoral Science Foundation (2025M782949), and the Natural Science Foundation of Yangzhou (YZ2025125).

Conflicts of Interest

The authors declare no conflict of interest.

Data Availability Statement

The data that support the findings of this study are available from the corresponding author upon reasonable request.

References

1. Z. Wang, Y. Dou, X. Yang, et al., "Global, Regional, and National Burden of Mental Disorders Among Adolescents and Young Adults, 1990–2021: A Systematic Analysis for the Global Burden of Disease Study 2021," *Translational Psychiatry* 15 (2025): 397, https://doi.org/10.1038/s41398-025-03623-w.

2. Y. Fan, A. Fan, Z. Yang, and D. Fan, "Global Burden of Mental Disorders in 204 Countries and Territories, 1990–2021: Results From the Global Burden of Disease Study 2021," *BMC Psychiatry* 25 (2025): 486, https://doi.org/10.1186/s12888-025-06932-y.

3. Z. Zhang, X. Chen, S. Wu, et al., "Global, Regional and National Burden of Anxiety and Depression Disorders From 1990 to 2021, and Forecasts up to 2040," *Journal of Affective Disorders* 393 (2026): 120299, https://doi.org/10.1016/j.jad.2025.120299.

4. Y. Huang, T. Loux, X. Huang, and X. Feng, "The Relationship Between Chronic Diseases and Mental Health: A Cross-Sectional Study," *Mental*

15214095, 0, Downloaded from https://advanced.onlinelibrary.wiley.com/doi/10.1002/adma.202532010 by Nanjing University, Wiley Online Library on [13/02/2026]. See the Terms and Conditions (https://onlinelibrary.wiley.com/terms-and-conditions) on Wiley Online Library for rules of use; OA articles are governed by the applicable Creative Commons License

Health & Prevention 32 (2023): 200307, https://doi.org/10.1016/j.mhp.2023.200307.

5. Y. Pu, L. Wang, H. Chen, et al., "Global, Regional and National Burden of Depression Among Adolescents and Young Adults Aged 15–39 Years, 1990–2021 and Projections to 2035: Findings From the Global Burden of Disease (2021) Study," *Journal of Psychiatric Research* 191 (2025): 438–453, https://doi.org/10.1016/j.jpsychires.2025.09.037.

6. D. Y. Jeong, S. Kim, M. J. Son, et al., "Induction and Maintenance Treatment of Inflammatory Bowel Disease: A Comprehensive Review," *Autoimmunity Reviews* 18 (2019): 439–454, https://doi.org/10.1016/j.autrev.2019.03.002.

7. J. T. Chang, "Pathophysiology of Inflammatory Bowel Diseases," *The New England Journal of Medicine* 383 (2020): 2652–2664, https://doi.org/10.1056/NEJMra2002697.

8. A. Lavelle and H. Sokol, "Gut Microbiota-Derived Metabolites as Key Actors in Inflammatory Bowel Disease," *Nature Reviews Gastroenterology & Hepatology* 17 (2020): 223–237, https://doi.org/10.1038/s41575-019-0258-z.

9. J. Halfvarson, C. J. Brislawn, R. Lamendella, et al., "Dynamics of the Human Gut Microbiome in Inflammatory Bowel Disease," *Nature Microbiology* 2 (2017): 17004, https://doi.org/10.1038/nmicrobiol.2017.4.

10. T. H. Bisgaard, K. H. Allin, L. Keefer, A. N. Ananthakrishnan, and T. Jess, "Depression and Anxiety in Inflammatory Bowel Disease: Epidemiology, Mechanisms and Treatment," *Nature Reviews Gastroenterology & Hepatology* 19 (2022): 717–726, https://doi.org/10.1038/s41575-022-00634-6.

11. F. S. Fousekis, A. H. Katsanos, G. Kourtis, et al., "Inflammatory Bowel Disease and Patients with Mental Disorders: What Do We Know?," *Journal of Clinical Medicine Research* 13 (2021): 466–473, https://doi.org/10.14740/jocmr4593.

12. A. A. Mikocka-Walus, D. A. Turnbull, N. T. Moulding, I. G. Wilson, J. M. Andrews, and G. J. Holtmann, "Controversies Surrounding the Comorbidity of Depression and Anxiety in Inflammatory Bowel Disease Patients," *Inflammatory Bowel Diseases* 13 (2006): 225–234, https://doi.org/10.1002/ibd.20062.

13. S. Kamath, E. Sokolenko, S. R. Clark, et al., "Distinguishing the Causative, Correlative and Bidirectional Roles of the Gut Microbiota in Mental Health," *Nature Mental Health* 3 (2025): 1137–1151, https://doi.org/10.1038/s44220-025-00498-0.

14. M. R. Aburto and J. F. Cryan, "Gastrointestinal and Brain Barriers: Unlocking Gates of Communication Across the Microbiota–Gut–Brain Axis," *Nature Reviews Gastroenterology & Hepatology* 21 (2024): 222–247, https://doi.org/10.1038/s41575-023-00890-0.

15. S. M. Collins, M. Surette, and P. Bercik, "The Interplay Between the Intestinal Microbiota and the Brain," *Nature Reviews Microbiology* 10 (2012): 735–742, https://doi.org/10.1038/nrmicro2876.

16. S. Vieujean, V. Jairath, L. Peyrin-Biroulet, et al., "Understanding the Therapeutic Toolkit for Inflammatory Bowel Disease," *Nature Reviews Gastroenterology & Hepatology* 22 (2025): 371–394, https://doi.org/10.1038/s41575-024-01035-7.

17. A. Mikocka-Walus, A. C. Ford, and D. A. Drossman, "Antidepressants in Inflammatory Bowel Disease," *Nature Reviews Gastroenterology & Hepatology* 17 (2020): 184–192, https://doi.org/10.1038/s41575-019-0259-y.

18. P. Persoons, S. Vermeire, K. Demyttenaere, et al., "The Impact of Major Depressive Disorder on the Short- and Long-Term Outcome of Crohn's disease Treatment With Infliximab," *Alimentary Pharmacology & Therapeutics* 22 (2005): 101–110, https://doi.org/10.1111/j.1365-2036.2005.02535.x.

19. Q. Li, L. Lin, C. Zhang, et al., "The Progression of Inorganic Nanoparticles and Natural Products for Inflammatory Bowel Disease," *Journal of Nanobiotechnology* 22 (2024): 17, https://doi.org/10.1186/s12951-023-02246-x.

20. L. Gao, J. Zhuang, L. Nie, et al., "Intrinsic Peroxidase-Like Activity of Ferromagnetic Nanoparticles," *Nature Nanotechnology* 2 (2007): 577–583, https://doi.org/10.1038/nnano.2007.260.

21. J. Wu, X. Wang, Q. Wang, et al., "Nanomaterials With Enzyme-Like Characteristics (Nanozymes): Next-Generation Artificial Enzymes (II)," *Chemical Society Reviews* 48 (2019): 1004–1076, https://doi.org/10.1039/C8CS00457A.

22. H. Wei, L. Gao, K. Fan, et al., "Nanozymes: A Clear Definition With Fuzzy Edges," *Nano Today* 40 (2021): 101269, https://doi.org/10.1016/j.nantod.2021.101269.

23. Y. Zhang, A. Khalique, X. Du, et al., "Biomimetic Design of Mitochondria-Targeted Hybrid Nanozymes as Superoxide Scavengers," *Advanced Materials* 33 (2021): 2006570, https://doi.org/10.1002/adma.202006570.

24. Y. Liu, Y. Cheng, H. Zhang, et al., "Integrated Cascade Nanozyme Catalyzes In Vivo ROS Scavenging for Anti-Inflammatory Therapy," *Science Advances* 6 (2020): abb2695, https://doi.org/10.1126/sciadv.abb2695.

25. F. Lei, Q. Huang, C. Zhang, Y. Lin, Y. Zhang, and F. Wang, "Pathogenesis Guided Application of Nanozymes in the Treatment of Inflammatory Bowel Disease," *Materials Today Bio* 33 (2025): 102008, https://doi.org/10.1016/j.mtbio.2025.102008.

26. S. Zhao, Y. Li, Q. Liu, et al., "An Orally Administered CeO_2@Montmorillonite Nanozyme Targets Inflammation for Inflammatory Bowel Disease Therapy," *Advanced Functional Materials* 30 (2020): 2004692, https://doi.org/10.1002/adfm.202004692.

27. S. Zhou, H. Cai, X. He, Z. Tang, and S. Lu, "Enzyme-Mimetic Antioxidant Nanomaterials for ROS Scavenging: Design, Classification, and Biological Applications," *Coordination Chemistry Reviews* 500 (2024): 215536, https://doi.org/10.1016/j.ccr.2023.215536.

28. X. Wang, C. Yu, Y. Li, M. Zhang, J. Zhang, and H. Wang, "Dietary Polysaccharides as Gut Health Regulators: Structural Characteristics and Regulatory Mechanism," *Trends in Food Science & Technology* 161 (2025): 105074, https://doi.org/10.1016/j.tifs.2025.105074.

29. X. Liu, S. Su, J. Yao, et al., "Research Advance About Plant Polysaccharide Prebiotics, Benefit for Probiotics on Gut Homeostasis Modulation," *Food Bioscience* 59 (2024): 103831, https://doi.org/10.1016/j.fbio.2024.103831.

30. X. Li, F. Jiang, M. Liu, et al., "Synthesis, Characterization, and Bioactivities of Polysaccharide Metal Complexes: A Review," *Journal of Agricultural and Food Chemistry* 70 (2022): 6922–6942, https://doi.org/10.1021/acs.jafc.2c01349.

31. Y. Su, Y. Liu, Y. Zhong, et al., "Coordination-Driven Self-assembly of Biomolecules and Metal Ions: Advances in Methodology and Applications," *Coordination Chemistry Reviews* 527 (2025): 216403, https://doi.org/10.1016/j.ccr.2024.216403.

32. J. Gao, Y. Liang, and P. Liu, "Along the Microbiota–Gut–Brain Axis: Use of Plant Polysaccharides to Improve Mental Disorders," *International Journal of Biological Macromolecules* 265 (2024): 130903, https://doi.org/10.1016/j.ijbiomac.2024.130903.

33. P. Batista, S. A. Cunha, T. Ribeiro, et al., "Fucoidans: Exploring Its Neuroprotective Mechanisms and Therapeutic Applications in Brain Disorders," *Trends in Food Science & Technology* 143 (2024): 104300, https://doi.org/10.1016/j.tifs.2023.104300.

34. Z. Wang, Z.-X. Wang, K.-F. Xu, et al., "A Metal–Polyphenol-Based Antidepressant for Alleviating Colitis-Associated Mental Disorders," *Advanced Materials* 37 (2025): 2410993, https://doi.org/10.1002/adma.202410993.

35. P. Li, Q. Xia, H. Zhang, et al., "Targeting Macrophage Glucose Metabolism: Polysaccharide-Iron Nanozyme-Mediated Reactive Oxygen Species/Iron Homeostasis Restoration Ameliorates Inflammatory Bowel Disease With Anemia Comorbidity," *Journal of Colloid and Interface Science* 700 (2025): 138357, https://doi.org/10.1016/j.jcis.2025.138357.

15214095, 0, Downloaded from https://advanced.onlinelibrary.wiley.com/doi/10.1002/adma.202532010 by Nanjing University, Wiley Online Library on [13/02/2026]. See the Terms and Conditions (https://onlinelibrary.wiley.com/terms-and-conditions) on Wiley Online Library for rules of use; OA articles are governed by the applicable Creative Commons License

36. H. I. Hamouda, T. Li, S. Shabana, A. H. Hashem, and H. Yin, "Advances in Fucoidan and Fucoidan Oligosaccharides: Current Status, Future Prospects, and Biological Applications," *Carbohydrate Polymers* 358 (2025): 123559, https://doi.org/10.1016/j.carbpol.2025.123559.

37. H. Molavi, "Cerium-Based Metal-Organic Frameworks: Synthesis, Properties, and Applications," *Coordination Chemistry Reviews* 527 (2025): 216405, https://doi.org/10.1016/j.ccr.2024.216405.

38. S. Zhang, J. Ermann, M. D. Succi, et al., "An Inflammation-Targeting Hydrogel for Local Drug Delivery in Inflammatory Bowel Disease," *Science Translational Medicine* 7 (2015): 300ra128–300ra128, https://doi.org/10.1126/scitranslmed.aaa5657.

39. E. O. Mensah, O. N. Kanwugu, P. K. Panda, and P. Adadi, "Marine Fucoidans: Structural, Extraction, Biological Activities and Their Applications in the Food Industry," *Food Hydrocolloids* 142 (2023): 108784, https://doi.org/10.1016/j.foodhyd.2023.108784.

40. F. M. A. Akl, M. M. El-Sheekh, M. E. M. Makhlof, and S. I. Ahmed, "Antimicrobial, Antidiabetic, Antiviral, and Antioxidant Activities of Fucoidan Extracted From the Brown Seaweed Padina Pavonica," *BMC Biotechnology* 25 (2025): 70, https://doi.org/10.1186/s12896-025-01004-1.

41. S. J. Dixon and B. R. Stockwell, "The Role of Iron and Reactive Oxygen Species in Cell Death," *Nature Chemical Biology* 10 (2014): 9–17, https://doi.org/10.1038/nchembio.1416.

42. B. G. Childs, M. Durik, D. J. Baker, and J. M. van Deursen, "Cellular Senescence in Aging and Age-Related Disease: From Mechanisms to Therapy," *Nature Medicine* 21 (2015): 1424–1435, https://doi.org/10.1038/nm.4000.

43. K. K.-L. Wu, X. Xu, M. Wu, et al., "MDM2 Induces Pro-Inflammatory and Glycolytic Responses in M1 Macrophages by Integrating iNOS-Nitric Oxide and HIF-1α Pathways in Mice," *Nature Communications* 15 (2024): 8624, https://doi.org/10.1038/s41467-024-53006-w.

44. T. Ma, G. Gan, J. Cheng, et al., "Engineered Probiotics Enable Targeted Gut Delivery of Dual Gasotransmitters for Inflammatory Bowel Disease Therapy," *Angewandte Chemie International Edition* 64 (2025): 202502588, https://doi.org/10.1002/anie.202502588.

45. H. He, Q. Qin, F. Xu, et al., "Oral Polyphenol-Armored Nanomedicine for Targeted Modulation of Gut Microbiota–Brain Interactions in Colitis," *Science Advances* 9 (2023): adf3887, https://doi.org/10.1126/sciadv.adf3887.

46. A. H. Miller, E. Haroon, and J. C. Felger, "Therapeutic Implications of Brain–Immune Interactions: Treatment in Translation," *Neuropsychopharmacology* 42 (2017): 334–359, https://doi.org/10.1038/npp.2016.167.

47. P. Zhou, Q. Sun, L. Huang, et al., "Dual-Targeting Mn@CeO_2 Nanozyme-Modified Probiotic Hydrogel Microspheres Reshape Gut Homeostasis in Inflammatory Bowel Disease," *ACS Nano* 19 (2025): 31619–31642, https://doi.org/10.1021/acsnano.5c08999.

48. A. Metwaly, S. Reitmeier, and D. Haller, "Microbiome Risk Profiles as Biomarkers for Inflammatory and Metabolic Disorders," *Nature Reviews Gastroenterology & Hepatology* 19 (2022): 383–397, https://doi.org/10.1038/s41575-022-00581-2.

49. J. Yang, P. Zheng, Y. Li, et al., "Landscapes of Bacterial and Metabolic Signatures and Their Interaction in Major Depressive Disorders," *Science Advances* 6 (2020): aba8555, https://doi.org/10.1126/sciadv.aba8555.

50. C. Xue, G. Li, Q. Zheng, et al., "Tryptophan Metabolism in Health and Disease," *Cell Metabolism* 35 (2023): 1304–1326, https://doi.org/10.1016/j.cmet.2023.06.004.

51. T.-T. Li, X. Chen, D. Huo, et al., "Microbiota Metabolism of Intestinal Amino Acids Impacts Host Nutrient Homeostasis and Physiology," *Cell Host & Microbe* 32 (2024): 661–675.e10, https://doi.org/10.1016/j.chom.2024.04.004.

52. M. Zhao, Z. Ren, A. Zhao, et al., "Gut Bacteria-Driven Homovanillic Acid Alleviates Depression by Modulating Synaptic Integrity," *Cell Metabolism* 36 (2024): 1000–1012.e6, https://doi.org/10.1016/j.cmet.2024.03.010.

53. N. Liu, J. He, Y. Yang, et al., "Enteric GABAergic Neuron-Derived γ-Aminobutyric Acid Initiates Expression of Igfbp7 to Sustain ILC3 Homeostasis," *Nature Immunology* 26 (2025): 404–415, https://doi.org/10.1038/s41590-025-02081-2.

Supporting Information

Additional supporting information can be found online in the Supporting Information section.

Supporting File: adma72370-sup-0001-SuppMat.docx.

15214095, 0, Downloaded from https://advanced.onlinelibrary.wiley.com/doi/10.1002/adma.202522010 by Nanjing University, Wiley Online Library on [13/02/2026]. See the Terms and Conditions (https://onlinelibrary.wiley.com/terms-and-conditions) on Wiley Online Library for rules of use; OA articles are governed by the applicable Creative Commons License